



Epitaxial Technologies for SiGeSn High Perf Optoelectronic Dev

**Baohua Li
ARKTONICS, LLC**

**04/29/2015
Final Report**

DISTRIBUTION A: Distribution approved for public release.

**Air Force Research Laboratory
AF Office Of Scientific Research (AFOSR)/ RTD
Arlington, Virginia 22203
Air Force Materiel Command**



ARKTONICS, LLC

April 20, 2015

Dr. Gernot Pomrenke, AFOSR/RTD
Air Force Office of Scientific Research
875 North Randolph Street, STE 325, Room 3112
Arlington, VA 22203
Email: gernot.pomrenke@us.af.mil

Dear Dr. Pomrenke,

Attached for your review is Final Technical Report covering the performance period of July 1, 2014 through March 31, 2015 with Contract Number FA9550-14-C-0044. Also attached are the required Material Inspection and Receiving Report, DD Form 250, and Invention Report, DD Form 882. Please contact me if you have any questions.

Sincerely,

Baohua Li
President
Arktonics, LLC
1339 S. Pinnacle Dr.
Fayetteville, AR 72701-7781
Email: Arktonics@gmail.com
Phone: 479-287-2406

REPORT DOCUMENTATION PAGE

Form Approved
OMB No. 0704-0188

The public reporting burden for this collection of information is estimated to average 1 hour per response, including the time for reviewing instructions, searching existing data sources, gathering and maintaining the data needed, and completing and reviewing the collection of information. Send comments regarding this burden estimate or any other aspect of this collection of information, including suggestions for reducing the burden, to the Department of Defense, Executive Service Directorate (0704-0188). Respondents should be aware that notwithstanding any other provision of law, no person shall be subject to any penalty for failing to comply with a collection of information if it does not display a currently valid OMB control number.

PLEASE DO NOT RETURN YOUR FORM TO THE ABOVE ORGANIZATION.

1. REPORT DATE (DD-MM-YYYY) 20-04-2015		2. REPORT TYPE Final Technical Report		3. DATES COVERED (From - To) July 2014-March 2015	
4. TITLE AND SUBTITLE (AF SBIR Phase I) Epitaxial Technologies for SiGeSn High Performance Optoelectronic Devices				5a. CONTRACT NUMBER FA9550-14-C-0044	
				5b. GRANT NUMBER	
				5c. PROGRAM ELEMENT NUMBER	
6. AUTHOR(S) Li, Baohua				5d. PROJECT NUMBER	
				5e. TASK NUMBER	
				5f. WORK UNIT NUMBER	
7. PERFORMING ORGANIZATION NAME(S) AND ADDRESS(ES) Arktonics, LLC 1339 S. Pinnacle Dr. Fayetteville, AR 72701				8. PERFORMING ORGANIZATION REPORT NUMBER	
9. SPONSORING/MONITORING AGENCY NAME(S) AND ADDRESS(ES) Program Manager/Officer: Dr. Gernot Pomrenke, AFOSR/RTD Air Force Office of Scientific Research 875 N. Randolph Street, STE 325 Room 3112 Arlington, VA 22203				10. SPONSOR/MONITOR'S ACRONYM(S) AA	
				11. SPONSOR/MONITOR'S REPORT NUMBER(S)	
12. DISTRIBUTION/AVAILABILITY STATEMENT "Distribution Statement A Approved for public release; distribution unlimited" (include waiver of STTR data rights on company letterhead signed by proper company authority)					
13. SUPPLEMENTARY NOTES					
14. ABSTRACT The report is developed under SBIR contract for topic AF141-002. It includes work of growth of mid-IR GeSn/SiGeSn materials using UHV-CVD, in-depth characterizations of GeSn materials, and development of GeSn mid-IR detectors and emitters. For material growth work, buffer free growth of Ge, SiGe, SiSn, GeSn, and SiGeSn on Si substrate has been demonstrated. Both SnCl4 and SnD4 are used as Sn precursors for the growth. For material characterization work, a variety of techniques have been used to study the materials and a direct bandgap Ge0.9Sn0.1 alloy has been identified. For device work, photoconductive detectors, photo diodes, avalanche photo diodes, and LEDs were fabricated. The high responsivity of 2.85 A/W at 1.55 μm has been achieved with a Ge0.9Sn0.1 photoconductor at 77 K, which is higher than that of market dominating Ge and InGaAs detectors. Temperature-dependent electroluminescence and power output from Ge/GeSn/Ge double heterostructure n-i-p surface and edge emitting LEDs have been studied. The peak power of 0.1 W for a 8% Sn surface emitting LED has been obtained. A low temperature optical pumping characterization system for edge-emitting lasers has been constructed and the preliminary testing was conducted.					
15. SUBJECT TERMS SBIR Report					
16. SECURITY CLASSIFICATION OF:			17. LIMITATION OF ABSTRACT	18. NUMBER OF PAGES	19a. NAME OF RESPONSIBLE PERSON
a. REPORT	b. ABSTRACT	c. THIS PAGE			Baohua Li
U	U	U	UU	38	19b. TELEPHONE NUMBER (Include area code) 479-287-2406

Abstract:

The main content of this report includes i) Growth of mid-IR GeSn/SiGeSn materials using Ultra-high-vacuum Chemical Vapor Deposition, ii) In-depth characterizations of GeSn materials using different techniques, and iii) Development of GeSn mid-IR detectors and emitters. For material growth work, **buffer free growth** of Ge, SiGe, SiSn, GeSn, and SiGeSn on Si substrate has been demonstrated. Both SnCl₄ and SnD₄ are used as Sn precursors for GeSn and SiGeSn growth. So far 276 wafers have been grown. The GeSn/SiGeSn material characterizations have been performed via X-ray diffraction, Raman, ellipsometry, Rutherford backscattering spectra (RBS), and high resolution transmission electron microscopy (TEM). The XRD result clearly shows GeSn, SiGe, and SiGeSn peaks indicating the success of the growth. The highest Sn incorporation is determined to be 7% for GeSn materials and the substitutional incorporation of Sn for SiGeSn varies from 2% to 5%. The reciprocal space map shows that the as-grown GeSn layers are relaxed. The TEM image shows that the misfit dislocations are localized at the interface between Si and epitaxy layer. Room temperature photoluminescence (PL) from GeSn and SiGeSn samples have been observed. The PL peak positions agree well with the theoretical prediction. High quality GeSn samples grown by ASM have been comprehensively characterized. A direct bandgap Ge_{0.9}Sn_{0.1} alloy has been identified which is **the first report of direct bandgap GeSn alloy**. Moreover, bandgap shrinkage has been observed in heavily doped n-type samples. GeSn samples have been fabricated into photoconductive detectors, avalanche photo diodes, and light-emitting diodes (LEDs) and in-depth study has been conducted. **The responsivity of 1.63 A/W at 1.55 μm** has been achieved with a Ge_{0.9}Sn_{0.1} photoconductor at 77 K, which is higher than that of market dominating Ge and InGaAs detectors. The team has done for **the first time a side by side comparison for specific detectivity (D*) between GeSn and other market dominating infrared detectors** in short wavelength infrared range. **An improved responsivity of 2.85 A/W** has been achieved on Ge_{0.9}Sn_{0.1} photoconductors at 1.55 μm and 77 K by using an interdigitated electrode design. Temperature-dependent electroluminescence and power output from Ge/GeSn/Ge double heterostructure n-i-p surface and edge emitting LEDs have been studied for samples with Sn composition up to 10%. **The peak emission power of 0.1 W** (8% Sn surface emitting LED at 800 A/cm² and 350 K) and 50 mW (8% Sn edge emitting LED at 1600 A/cm² and 300 K) have been achieved, respectively. An optical pumping characterization system for edge-emitting lasers has been constructed and the preliminary results from a 11% GeSn sample have been obtained showing the promise of achieving lasing at low temperatures.



I. Material growth and characterization of mid-IR Si-Ge-Sn material system by UHV-CVD

GeSn alloys have been grown directly on Si substrate at low temperatures using two different Sn precursors (SnCl₄ and SnD₄) via a cold-wall ultra-high-vacuum chemical-vapor-deposition system (UHV-CVD). Moreover, growth of SiGeSn alloys has been successfully demonstrated. In-depth material characterization has been conducted. A list of work performed by Arktonics, LLC and University of Arkansas (UA) as a team in the phase I period and highlights of results are given below.

- Both SnCl₄ and SnD₄ as Sn precursors are used for GeSn and SiGeSn growth (The only team in the world demonstrated such growth capability for both precursors);
- No buffer layer needed during the GeSn growth (First demonstration in the world using these precursors, see Table I for the uniqueness of this work);
- GeSn alloys have been successfully grown on Si with Sn composition up to 7%;
- Growth of SiSn and SiGe have been demonstrated; Material characterization of SiGe have been conducted;
- Growth of SiGeSn has been demonstrated. The incorporation of Si and Sn in Ge has been identified (see Table II for all sample growth summary);
- Detailed material characterizations of GeSn and SiGeSn have been conducted;
- PL spectra of GeSn and SiGeSn samples with different Sn compositions have been obtained;
- GeSn photoconductor device has been fabricated and the device shows room temperature photo response;
- Totally **276** rounds of growth have been done.

Table I A brief summary of material growth using CVD methods by different research groups

Growth team	Growth system	Ge precursor	Sn precursor	Carrier gas	Buffer layer	SiGeSn growth
Arizona State University	UHV-CVD	Different chemistries	SnD ₄	H ₂	No	Yes
ASM/UA	RP-CVD	GeH ₄	SnCl ₄	N ₂ /H ₂	Ge	Yes
IMEC	AP-CVD	Ge ₂ H ₆	SnCl ₄	N ₂ /H ₂	Ge	No
Applied Materials	RP-CVD	Ge ₂ H ₆	SnCl ₄	Ar/N ₂ /H ₂	Ge	No
Peter Grünberg Institute	RP-CVD	Ge ₂ H ₆	SnCl ₄	Ar/H ₂	No	Yes
Translucent	Hot wall UHV-CVD	GeH ₄	SnD ₄	N. A.	No	Yes
UA/Arktonics	Cold wall UHV-CVD	GeH₄	SnCl₄/SnD₄	No	No	Yes

Table II A brief summary of material growth for Ge, SiGe, SiSn, GeSn, and SiGeSn by UA/Arktonics

Epitaxy layer	Ge	SiGe	SiSn	GeSn		SiGeSn	
Precursors	GeH ₄	SiH ₄ , GeH ₄ , Ar	SiH ₄ , SnCl ₄	GeH ₄		SiH ₄ , GeH ₄	
Sn precursor				SnCl ₄	SnD ₄	SnCl ₄	SnD ₄
Number of round (Jul.~Sep. 2014)	40	10	10	40	0	15	0
Number of round (Oct.~Dec. 2014)	5*	34	0	2	34	12	22
Number of round (Jan.~Mar. 2015)	4**	0	0	43	5	0	0
Total Number of round	49	44	10	85	39	27	22

* Using Ar as carrier gas. ** Using N₂ as carrier gas.



i) Growth and characterization of GeSn

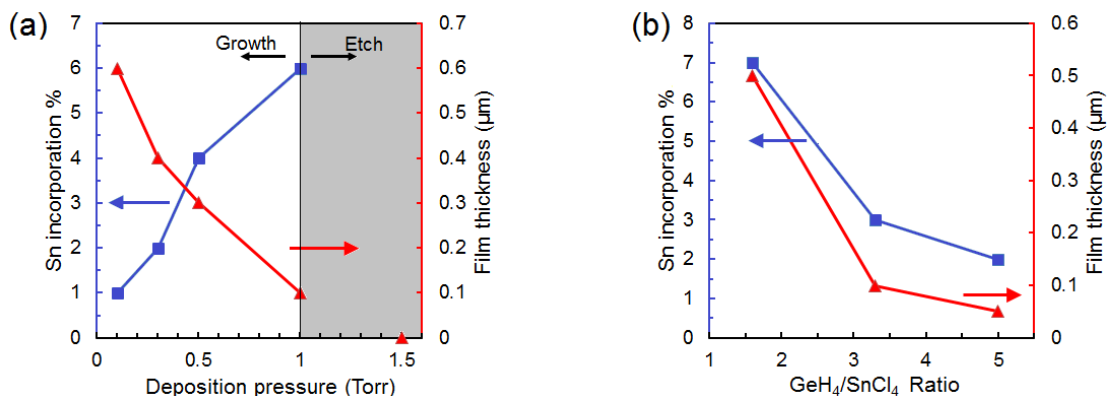


Fig. 1. (a) Sn incorporation percentage and film thickness as the functions of deposition pressure. The fixed gas flow ratio of GeH₄/SnCl₄=1.6. Films were etched off when pressure was higher than 1 Torr. (b) Sn incorporation percentage and film thickness as the functions of gas flow ratio. The fixed deposition pressure is 0.5 Torr.

The study of growth mechanism using SnCl₄ and GeH₄ as precursors for GeSn deposition has been conducted. Fig. 1(a) shows the GeSn thin films grown on Si at different pressures. Growth starts happening from 0.1 Torr and continues until the pressure reaches 1 Torr. When the pressure is higher than 1 Torr, the films are etched off. Fig. 1(b) shows GeSn growth results at different gas flow ratios of GeH₄/SnCl₄. The pressure is fixed at 0.5 Torr. A paper reporting the growth results and the growth mechanism currently has been accepted in *Frontiers in Materials (In Press)*.

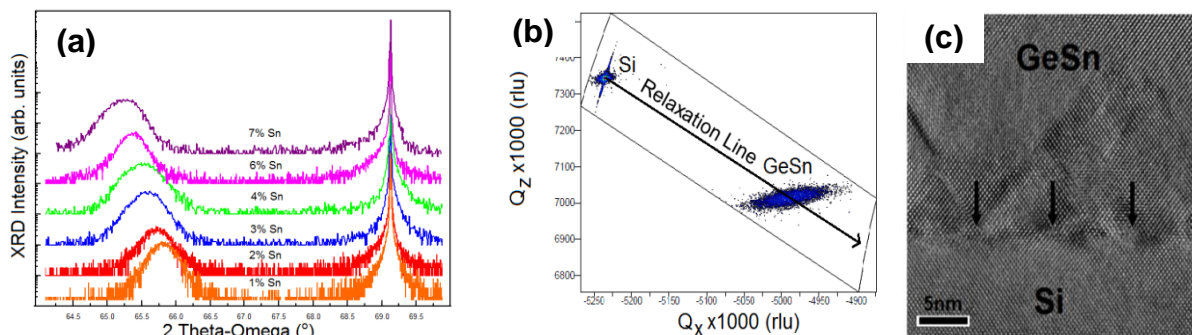


Fig. 2. (a) Symmetric (0 0 4) 2θ-ω scan of GeSn films. The peak at 69° is attributed to Si substrate and the peaks between 66-65° belong to GeSn films. (b) Reciprocal space map (RSM) from asymmetrical plane (-2 -2 4) for Ge_{0.94}Sn_{0.06}. The RSM shows that the film is strain relaxed on Si substrate. (c) TEM images of Ge_{0.94}Sn_{0.06} film. The arrows show misfit dislocations formed at GeSn/Si interface due to the large lattice mismatch between Si and GeSn.

Material characterization results are summarized in Fig. 2. Analysis of Sn mole fraction, lattice constant, growth quality and strain in the GeSn films has been performed using high resolution X-ray diffraction (HRXRD) and high resolution transmission electron microscopy (TEM). In Fig. 2(a), the gradual shift of GeSn peaks in HRXRD indicates the increase of Sn composition. The results show GeSn with Sn compositions from 1% to 7% (Note, the sample with 5% Sn is not shown due to low quality). In Fig. 2(b), the RSM shows that the GeSn layer is strain relaxed grown on Si substrate. In Fig. 2(c), the TEM image shows that the misfit dislocations are localized at GeSn/Si interface.



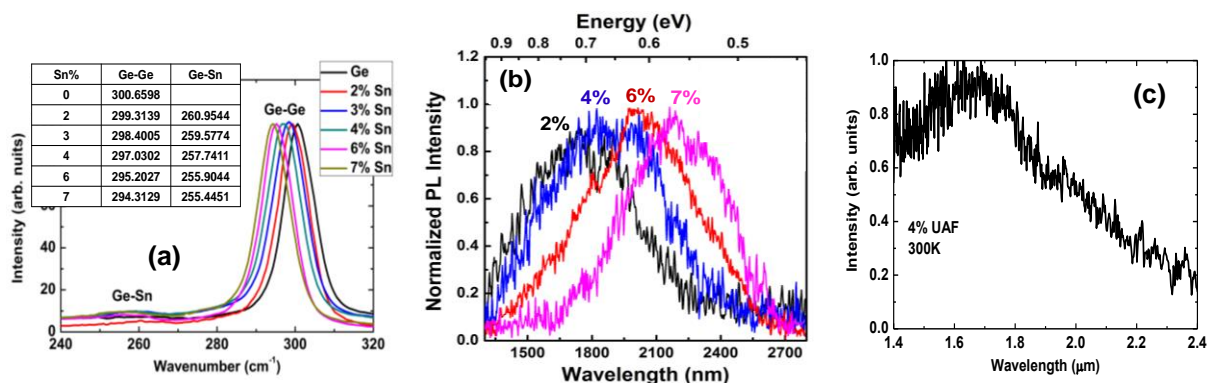


Fig. 3. (a) Raman spectra of the GeSn films. The shift in Ge-Ge peak results from the incorporation of Sn in Ge lattice which changes the bond size of Ge-Ge lattice. Ge-Sn peaks are shown at lower wavenumber due to a weaker bond. (b) Room temperature photoluminescence spectra of the GeSn films with Sn compositions of 2, 4, 6, and 7%. Incorporation of Sn has shifted bandgap towards lower energies. (c) Room temperature photoconductor spectrum response for a device fabricated using a 4% GeSn sample grown by UA.

Optical characterization of the GeSn samples has been performed using Raman and photoluminescence (PL) spectroscopy as shown in Fig. 3(a) and (b), respectively. Fig. 3(a) shows that the Ge-Ge peak in the GeSn films are shifted to lower wavenumbers due to the induced strain by incorporation of Sn atoms. The Ge-Sn peaks for different Sn mole fractions are observed at 250-260 cm^{-1} also shown in the figure. Fig. 3(b) shows the normalized PL emission for different samples. From the spectrum, it is clear that as Sn composition increases, the PL peak shifts toward to longer wavelength as a result of bandgap energy reduction. The sample with 4% Sn has been fabricated into photoconductor devices with our previously developed process. The device spectrum response at 300K is shown in Fig. 3(c) with response going beyond standard Ge detector long wavelength cut-off and extending to 2.4 μm . The longer wavelength response beyond the material bandgap is attributed to thermal effect and defects.

The team has conducted study of GeSn growth using SnD_4 as Sn precursor. Since SnD_4 is fairly unstable at the room temperature, the vendor (Voltaix) initially could not guarantee the gas quality. The team has come out a solution to obtain the SnD_4 with a low temperature package, which could maintain it to be chemically stable but it is in liquid phase. A special gas cabinet was built with a Dewar (filled with dry ice) to bring the SnD_4 cylinder to around -50°C so that a stable vapor gas pressure could be maintained. Then Argon gas was brought in to mix with SnD_4 and the mixed gases were delivered to the growth chamber through a mass flow controller (MFC). This gas delivery method is different from what Arizona State University used for their GeSn growth and is more manufacture friendly.

Due to the fast decomposition of SnD_4 in the delivery line and MFC walls, the flow rate readings are not accurate. Therefore, a pressure-based system is adopted for accurate measurement of SnD_4 flow as well as all other precursors and Ar. The deposition pressure of the system is controlled by a throttle valve which is placed before the turbo-pump. In order to calibrate the flow rates with the deposition pressure in the system, the throttle valve is place at different positions and the flow rates of the gases can be changed. For example, at 1% open position of the throttle valve, the flow rate of Ar has changed from 1 to 25 sccm and the corresponding pressure has been recorded. The same procedure has been adopted for germane and silane. The partial pressures of all gases are measured by capacitance monometer pressure gauge in the vacuum chamber. In order to determine the partial pressure of SnD_4 a needle valve is placed on the delivery line to control the gas flow in the chamber (Figure 4). In addition, SnD_4 is kept in the temperature around -50°C to maintain its liquid form. The vapor pressure of the gas is led to the chamber through a needle valve. By opening the needle valve at different positions, the partial pressure of the gas is controlled from 0 to 1.5 mTorr. After recording all the partial pressures for different gases, the chamber is set to the desired pressure and temperature the experiments are carried out under different

conditions. The typical temperature range was set to 300-450 °C and the deposition pressure was kept between 0.1 to 10 Torr. Using this method, SnD₄ purchased from Voltaix could be used to up to three months. The team initially submitted an invention disclosure for this technique, but eventually withdrew it after careful consideration because the team feels that there is still a lot of room to improve the setup for much more accurate control of gas delivery.

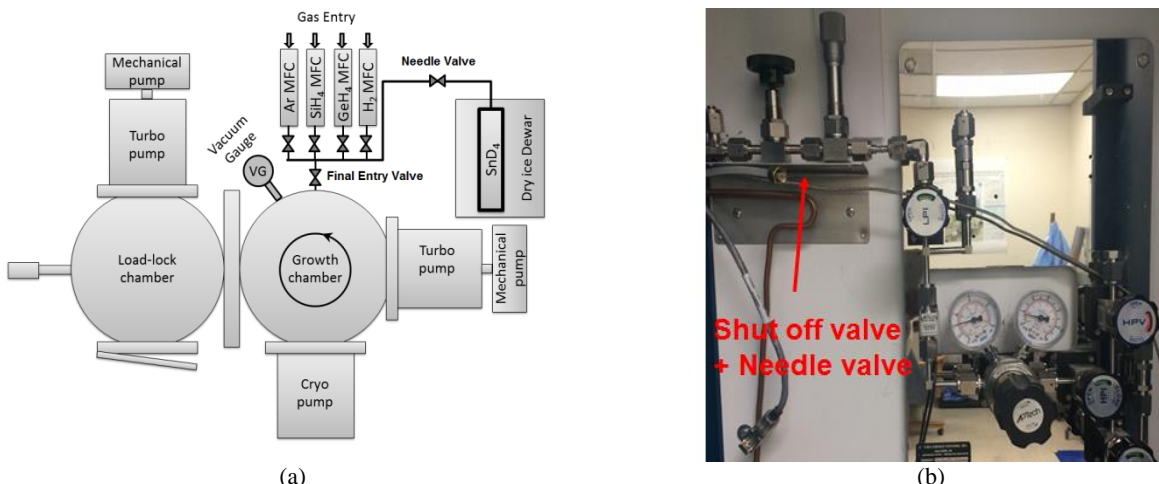


Fig. 4. (a) Cold wall UHV-CVD system with SnD₄ in-situ gas mixing. The samples are loaded in the load-lock chamber and after pumping down to 10⁻⁸ Torr pressure it is transferred to the growth chamber. The growth chamber is pumped down with a turbo-molecular pump and a cryogenic pump. Gases are entered in the chamber through a MFC and a final entry valve. The SnD₄ gas is kept in dry ice Dewar and the vapor pressure is mixed with the gases before entering the chamber through a needle valve. Partial pressure of SnD₄ gas as well as silane, germane, and argon are measured by a vacuum gauge. (b) The needle valve is placed after the gas regulators in order to control the SnD₄ flow.

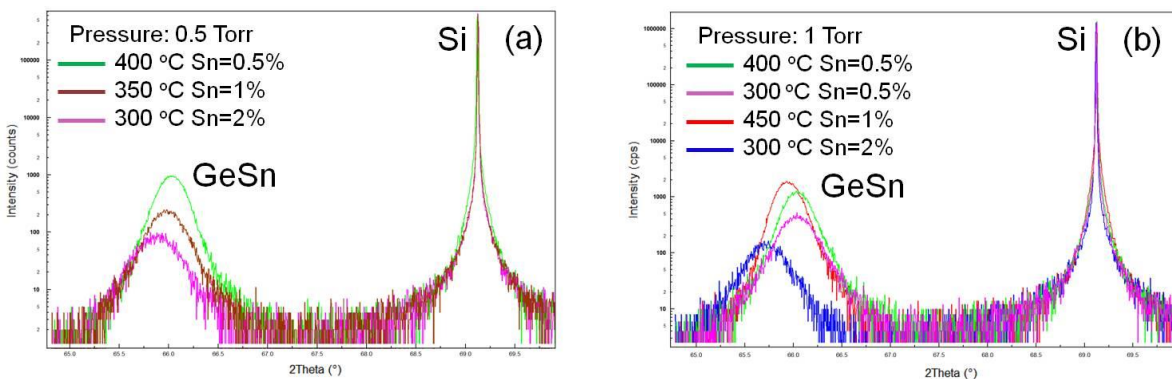


Fig. 5. 2θ-ω scan of GeSn using SnD₄ as Sn precursor. Material growth at different temperatures at the pressure of (a) 0.5 Torr and (b) 1 Torr. The GeSn peak shifts to lower angle as Sn composition increases.

Analysis of Sn mole fraction and growth quality of the GeSn films has been performed using high resolution X-ray diffraction (HRXRD). Fig. 5(a) and (b) show the 2θ-ω scan of GeSn thin films grown on Si at the pressures of 0.5 and 1 Torr using SnD₄, respectively. The growth temperature was also shown in the figures, which was kept below 450 °C to be compatible with a Si complementary metal-oxide-semiconductor (CMOS) process. The GeSn peaks shift toward lower angle in HRXRD indicating the increase of Sn composition. The growth has been conducted with chamber pressure from 0.1 to 1 Torr. The GeSn growth does not require a prior growth of a Ge buffer layer.



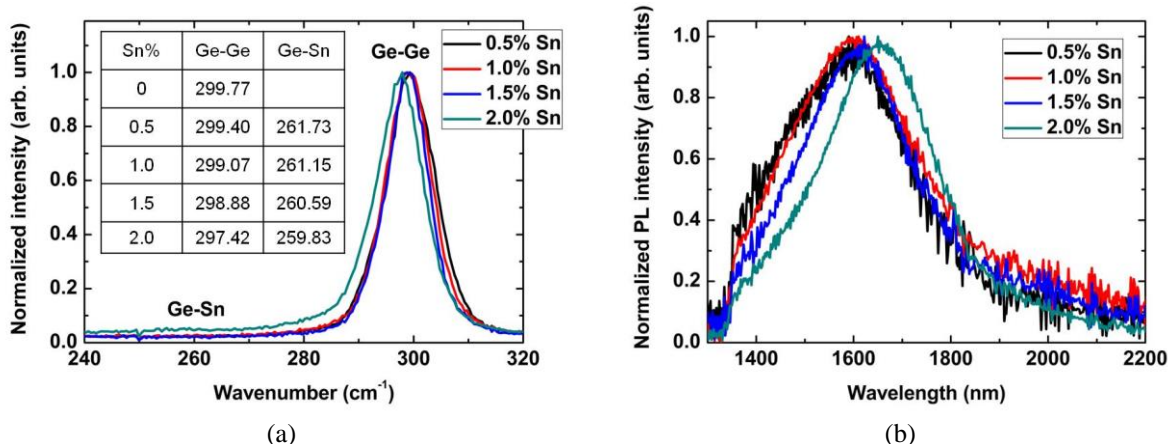


Fig. 6. (a) Raman spectra of the GeSn films. The shift in Ge-Ge peak is due to the incorporation of Sn in Ge lattice which changes the bond size of Ge-Ge lattice. Ge-Sn peaks are shown at lower wavenumber due to a weaker bond. Inset: peak positions of Ge-Ge and Ge-Sn. (b) Room temperature photoluminescence spectra of the GeSn films with Sn compositions from 0.5 to 2%. Incorporation of Sn has reduced the bandgap energy and therefore shifted the PL peak from 1583 nm (0.5% Sn) to 1648 nm (2% Sn).

Optical characterization of the GeSn samples has been performed using Raman and photoluminescence (PL) spectroscopy as shown in Fig. 6(a) and (b), respectively. In Fig. 6(a), the Ge-Ge peaks in the GeSn films are shifted toward lower wavenumbers due to the induced strain by incorporation of Sn atoms. The Ge-Sn peaks also shift toward lower wavenumbers as Sn composition increases. The summarized peak positions are shown in Fig. 6(a) inset. Fig. 6(b) shows the normalized PL emission from GeSn films with Sn compositions from 0.5 to 2%. As Sn composition increases, the PL peak shifts toward longer wavelength as a result of bandgap energy reduction.

ii) Growth and characterization of SiGe

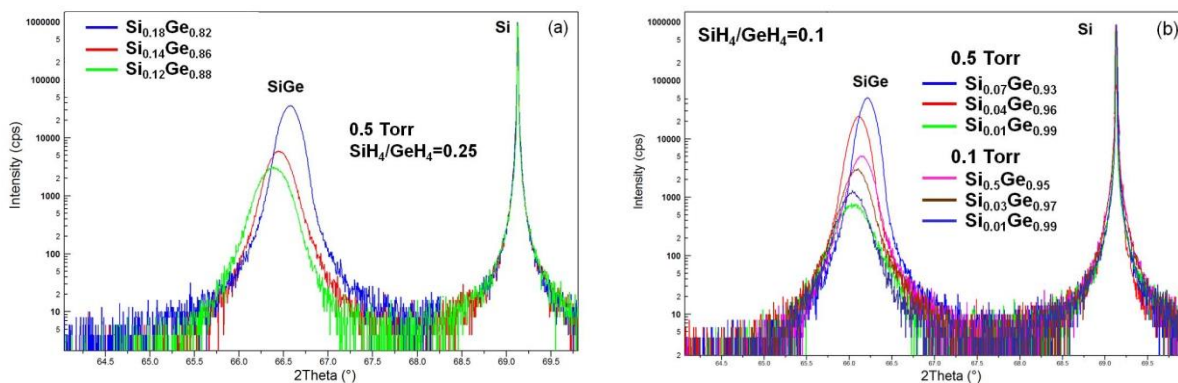


Fig. 7. 2θ - ω scan of SiGe. (a) $\text{SiH}_4/\text{GeH}_4=0.25$ and pressure of 0.5 Torr. (b) $\text{SiH}_4/\text{GeH}_4=0.1$ and pressure of 0.5 and 0.1 Torr.

In order to demonstrate growth of SiGeSn, the study of SiGe growth was firstly conducted (followed by the Sn incorporation to finally achieve SiGeSn growth). The growth mechanism has been investigated and the results are summarized below. Figure 7 shows the 2θ - ω scan of SiGe thin films. At high $\text{SiH}_4/\text{GeH}_4$ ratio of 0.25, the Si compositions are from 12 to 18%, as shown in Fig. 7(a). At low $\text{SiH}_4/\text{GeH}_4$ ratio of 0.1, the Si composition varies from 1 to 5% at pressure of 0.1 Torr and from 1 to 7% at pressure of 0.5 Torr, respectively, as shown in Fig. 7(b). Increase in $\text{SiH}_4/\text{GeH}_4$ ratio and chamber pressure results in higher Si incorporation. Furthermore, the Si composition increases as growth temperature increases. All growth temperatures in this study were kept below 450 °C.



iii) Growth and characterization of SiGeSn

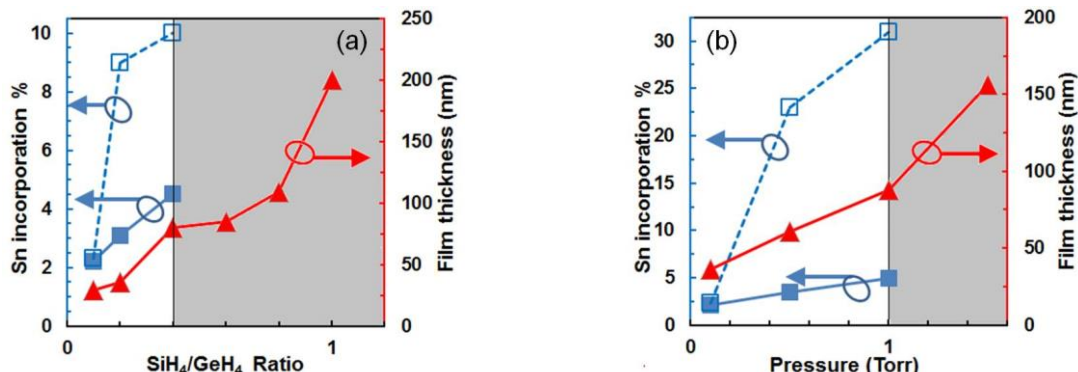


Fig. 8. SiGeSn growth mechanism. (a) Sn incorporation percentage and film thickness as the functions of gas flow ratio. The fixed deposition pressure is 0.1 Torr and the fixed ratio of SnCl₄/GeH₄ is 0.2. (b) Sn incorporation percentage and film thickness as the functions of deposition pressure. The fixed gas flow ratio of SiH₄/GeH₄/SnCl₄=2/10/1. The solid and dashed lines show substitutionally incorporated Sn and total incorporated Sn in SiGe lattice, respectively.

The growth of SiGeSn has been successfully demonstrated. The SiH₄, GeH₄, and SnCl₄ are used as Si, Ge, and Sn precursors, respectively. The study of growth mechanism has been conducted, as shown in Fig. 8. Fig. 8(a) shows the SiGeSn growth at different SiH₄/GeH₄ ratios. The pressure is fixed at 0.1 Torr and SnCl₄ flow was fixed as SnCl₄/GeH₄=0.2. Increase in SiH₄ flow results in increase in Sn incorporation. The solid and dashed lines show substitutionally incorporated Sn and total incorporated Sn in SiGe lattice, respectively. The deviation of two curves indicates that part of Sn interstitially incorporated into the SiGe lattice. Fig. 8(b) shows SiGeSn growth results at different chamber pressures. The fixed gas flow ratio is of SiH₄/GeH₄/SnCl₄=2/10/1. Increase in chamber pressure results in higher Sn incorporation in the film. Growth starts at 0.1 Torr and continues until the pressure reaches 1 Torr. When the pressure is higher than 1 Torr, the films become amorphous.

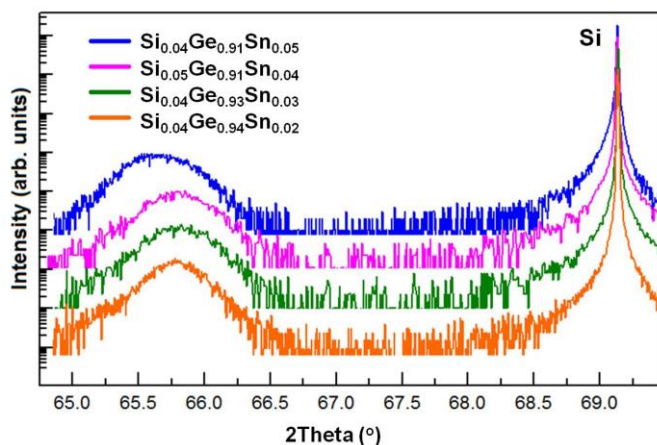


Fig. 9. 2θ-ω scan of SiGeSn films using SnCl₄ as Sn precursor. The peak at 69° is attributed to Si substrate and the peaks between 66.5-65° belong to SiGeSn films.

Figure 9 shows the 2θ-ω scan of SiGeSn thin films using SnCl₄ as Sn precursor with Sn compositions from 2 to 5 %. The Si composition was kept as 4 % (except a little higher one in Si_{0.05}Ge_{0.91}Sn_{0.04}). As Sn composition increases, the SiGeSn peak gradually shifts toward lower angle. Compared to GeSn samples



(the same Sn composition), these peaks are closer to the Si peak due to the Si incorporation. Therefore the incorporation of Si and Sn in Ge can be identified by the spectra behavior abovementioned.

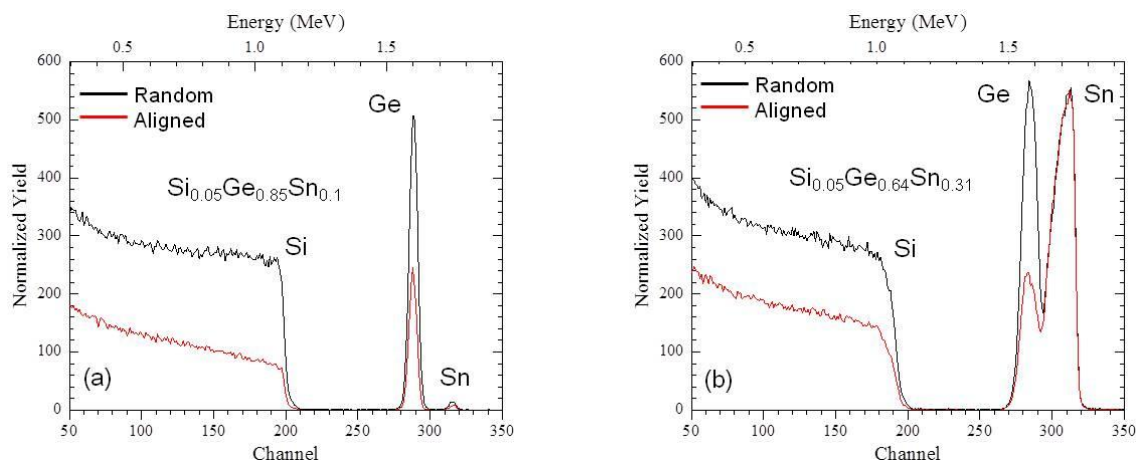


Fig. 10. Rutherford backscattering (RBS) spectra for (a) $\text{Si}_{0.05}\text{Ge}_{0.85}\text{Sn}_{0.1}$ and (b) $\text{Si}_{0.05}\text{Ge}_{0.64}\text{Sn}_{0.31}$. The black and red curves are random and aligned spectra, respectively.

Rutherford backscattering (RBS) spectra were used to identify the elemental content. Two representative SiGeSn samples are shown in Fig. 10. The black and red curves are random and aligned spectra, respectively. The ratios of peak heights for Si and Ge indicate that Si occupies substitutional lattice sites. On the other hand, the ratio of Sn peak heights reveals that not all of Sn atoms are substitutionally incorporated; some of them are interstitially incorporated into the SiGe lattice. The total incorporated Sn compositions shown in Fig. 10 are 10% and 31%, respectively. According to XRD measurement results, the corresponding substitutionally incorporated Sn compositions are 4% and 5%, respectively. The material quality needs to be further improved. The work of optimizing the growth condition is currently underway.

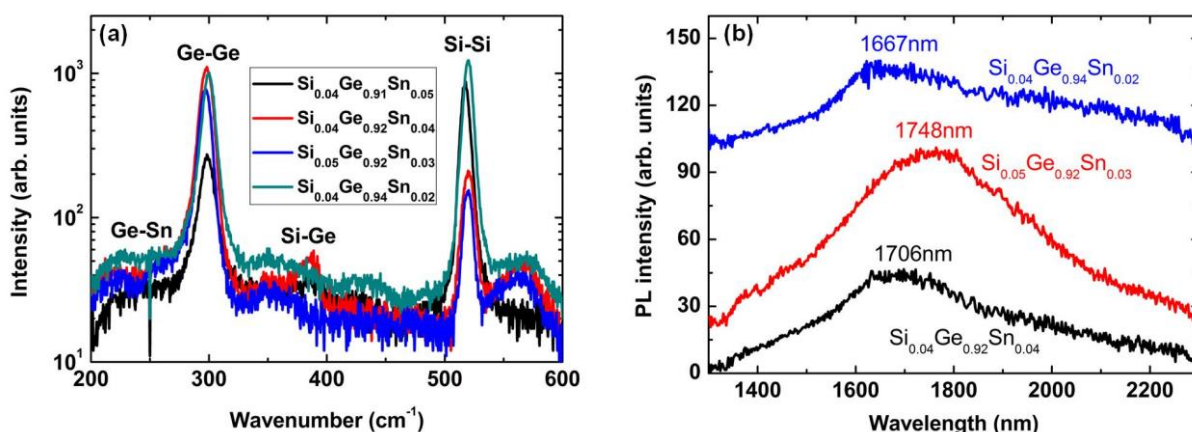


Fig. 11. (a) Raman spectra of the SiGeSn films. (b) Room temperature PL emissions from SiGeSn samples. Each spectrum is stacked for clarity.

Figure 11(a) shows the Raman spectra of the SiGeSn films. The shifts in Si-Si and Ge-Ge bonds are due to the incorporation of Si and Sn in the Ge lattice. The Si-Ge peaks are located between the Si-Si and Ge-Ge peaks and the Ge-Sn peaks are shown at lower wavenumbers than the Ge-Ge peaks. The peak

positions are summarized in Table III. Some Si-Ge and Ge-Sn peaks cannot be identified due to the low intensity in Raman spectra.

Table III Peak positions of Si-Si and Ge-Ge extracted from Fig. 11(a)

Sample	Si-Si	Ge-Ge	Si-Ge	Ge-Sn
Reference	522.357	300.006		
Si _{0.04} Ge _{0.91} Sn _{0.05}	520.526	297.588	399.096	
Si _{0.04} Ge _{0.92} Sn _{0.04}	520.156	297.861	398.735	259.538
Si _{0.05} Ge _{0.92} Sn _{0.03}	519.723	297.895		259.965
Si _{0.04} Ge _{0.94} Sn _{0.02}	519.876	299.695		260.006

Room temperature PL emissions from SiGeSn samples are shown in Fig. 11(b). Each spectrum is stacked for clarity. The incorporation of Sn reduces the bandgap energy, which on the contrary is increased by the incorporation of Si. Therefore the PL peak position is determined by both Si and Sn compositions.

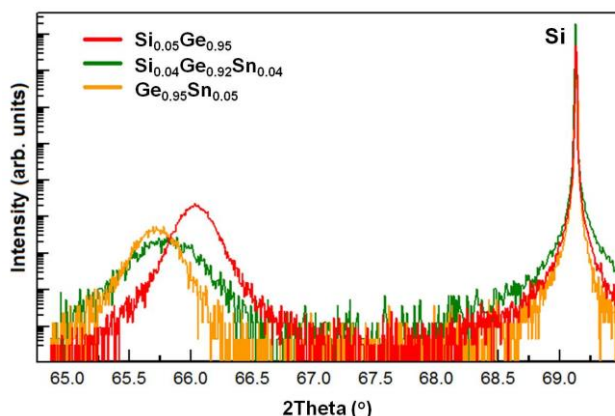


Fig. 12. Comparison of 2θ-ω scans between SiGe, SiGeSn, and GeSn samples. The incorporating of Si in the film shifts the peak toward to Si substrate peak, while incorporating of Sn shifts the peak away from the Si substrate peak, which agrees well with theoretical study.

Figure 12 shows the comparison of 2θ-ω scans between SiGe, SiGeSn, and GeSn samples. It is clear that the Si and Sn compositional-dependent peak positions agree well with theoretical predication.

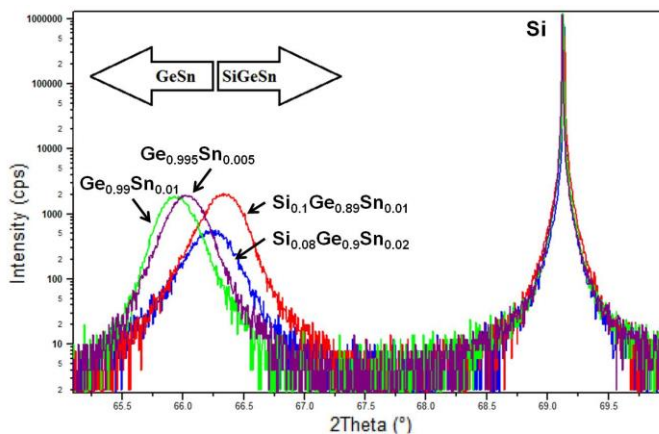


Fig. 13. 2θ - ω scan of SiGeSn and GeSn films. The peak positions follow the theoretical study.

The team has also conducted preliminary study of SiGeSn growth using SnD_4 as Sn precursor. The 2θ - ω scans of SiGeSn and GeSn films using SnD_4 as Sn precursor are shown in Fig. 13. The change of the peak positions follows the theoretical prediction. A paper reporting the growth results and the growth mechanism of GeSn and SiGeSn using SnD_4 as Sn precursor is under preparation.

II. In-depth study of GeSn optical characteristics

The GeSn samples from UA's collaborator ASM have been grown using an ASM Epsilon[®] 2000 Plus reduced pressure chemical vapor deposition system (RP-CVD). Detailed PL study has been conducted with a summary given in below.

- PL spectra of unintentionally doped GeSn samples with Sn composition from 1 to 10% with 1% increment have been obtained at room temperature (Fig. 14);
- Temperature-dependent PL study on GeSn films has been conducted to investigate the peak competing between direct and indirect bandgap transitions;
- A direct bandgap $\text{Ge}_{0.9}\text{Sn}_{0.1}$ alloy has been experimentally identified (Fig. 15, first demonstration of GeSn in the world);
- PL peaks of n-type doped samples have been investigated (Fig. 16, 11% Sn has shown PL emission at 2400 nm, the longest one reported in the world);
- Bandgap shrinkage has been observed in heavily doped n-type samples;
- Temperature dependent PL study on n-type doped samples has been conducted. The increased PL intensity at low temperature has been observed.

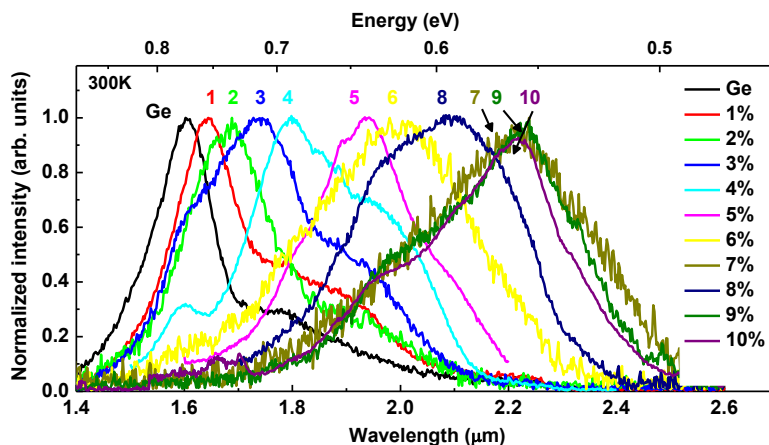


Fig. 14. Room temperature PL emissions from unintentionally doped GeSn samples with Sn compositions from 1 to 10%.

Figure 14 shows the PL spectra of GeSn samples with Sn compositions from 1 to 10% at room temperature. As Sn content increases, the PL peak shifts toward longer wavelength, indicating the narrowed bandgap due to Sn incorporation. The bandgap energy is also affected by strain, therefore 7% Sn sample shows narrower bandgap than 8% Sn sample because of the higher compressive strain of 8% Sn sample. At low Sn composition, two peaks corresponding to direct and indirect bandgap transitions can be identified clearly because of the sufficient energy separation. At higher Sn composition, these two peaks cannot be identified due to the reduced bandgap energy difference, resulting in only a single peak to be observed.



Temperature-dependent PL study on GeSn films with Sn compositions of 0.9, 3.2, and 6.0% has been conducted to investigate the peak competing between direct and indirect bandgap transitions, as shown in Fig. 15 (a), (b), and (c), respectively. In (a) and (b), two emission peaks in PL spectra can be clearly seen at 300 K. The high energy peaks are attributed to the direct band transition, while the lower energy peaks are ascribed to the indirect band transition. The energy differences which reflect the Γ - and L-valley separation are lower than that in Ge due to the incorporation of Sn. At 300 K, the PL intensity of direct transition is stronger than that of indirect transition because of the thermal excitation of electrons into the higher Γ -valley albeit still a small fraction of electrons occupying the Γ -valley – a direct result of strong radiative recombination of direct bandgap transition. The PL intensity of the indirect peak, on the other hand, is weaker at 300 K because of the less efficient phonon-assisted indirect radiative recombination. The PL intensity decreases as the temperature decreases with more rapid drop of the direct peak than the indirect peak. At 225 K, the direct peak almost disappears while the indirect peak is still recognizable, and as temperature decreases further the indirect transition completely dominates the PL. This can be explained by the fact that less electron occupation of the Γ -valley as the result of reduced thermal excitation from the lower L-valley at lower temperature. In Figure 15(c), since the peak energy difference of direct and indirect transition is small, the two peaks are mostly overlapped. At 300 and 275 K, the main peaks are attributed to the direct transition, while the indirect peaks almost disappear, indicating the direct transition dominates the PL at high temperature. As temperature decreases, the high energy direct peak drops more rapidly than the low energy indirect peak, and the direct peak was not observed when temperature is lower than 100 K (data not shown here), implying the indirect transition becomes the dominating the PL at low temperature.

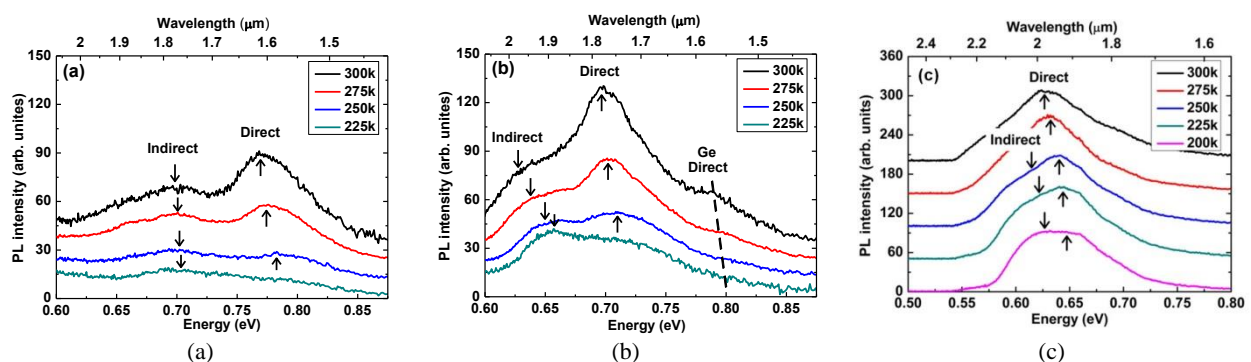


Fig. 15 Temperature-dependent PL spectra of (a) 0.9 % Sn sample; (b) 3.2 % Sn sample; and (c) 6 % Sn sample. Each curve is stacked for clarity. The direct peaks are marked by upwards arrows, while downward arrows indicate the indirect peaks.

A direct bandgap $\text{Ge}_{0.9}\text{Sn}_{0.1}$ alloy has been identified by temperature-dependent PL study based on the single peak spectrum and the narrow line-width. Room temperature PL emission as long as 2230 nm has also been observed from the same sample. In Fig. 16(a), the indirect and direct regions correspond to the indirect and direct bandgap materials, respectively. The uncertain region reveals the discrepancy of theoretical calculations due to various models and fitting parameters. Materials located in the uncertain region could be either direct or indirect bandgap material. The insets in indirect and direct regions show the schematic band diagrams of $\text{Ge}_{1-x}\text{Sn}_x$ alloy and the mechanism of PL spectra formation for indirect and direct bandgap materials, respectively. Fig. 16(b) shows temperature dependent PL spectra of a 10% GeSn sample in which only a single peak with narrowed line-width was observed. This PL linewidth reduction compared with that of lower Sn composition PL (for example 8 and 9%, not shown in this result) in combining with the PL linewidth forming mechanism shown in Fig. 16(a) indicating the 10% GeSn is a direct bandgap material. In Fig. 16(c), the line-width of 8 and 9 % Sn samples are nearly twice that of 10% Sn sample at the temperature range from 300 to 100 K, confirming that sample D is a direct bandgap material. In Fig. 16(d), region (i) and (ii) correspond to indirect bandgap material, while region (iii) corresponds to direct bandgap material. The solid and open symbols represent the direct and indirect bandgap energies, respectively. The 10% Sn sample is located in region (iii), which is determined as a

direct bandgap material. The solid and dashed lines are eye guidance of direct and indirect bandgap energies, respectively.

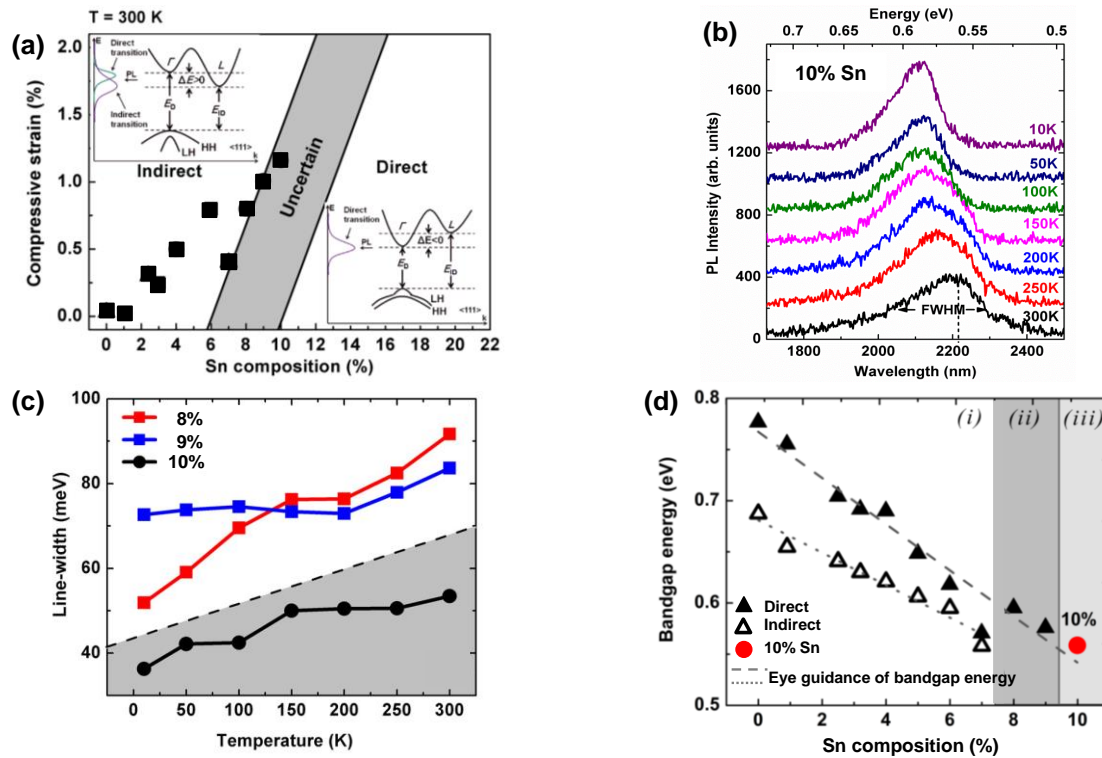


Fig. 16. (a) The effect of compressive strain and Sn composition in the indirect-to-direct bandgap transition at room temperature. (b) Temperature-dependent PL spectra of 10% Sn sample. (c) The line-width of the PL peaks as a function of temperature for samples with Sn compositions of 8, 9 and 10%. (d) Sn composition-dependent bandgap energies at room temperature.

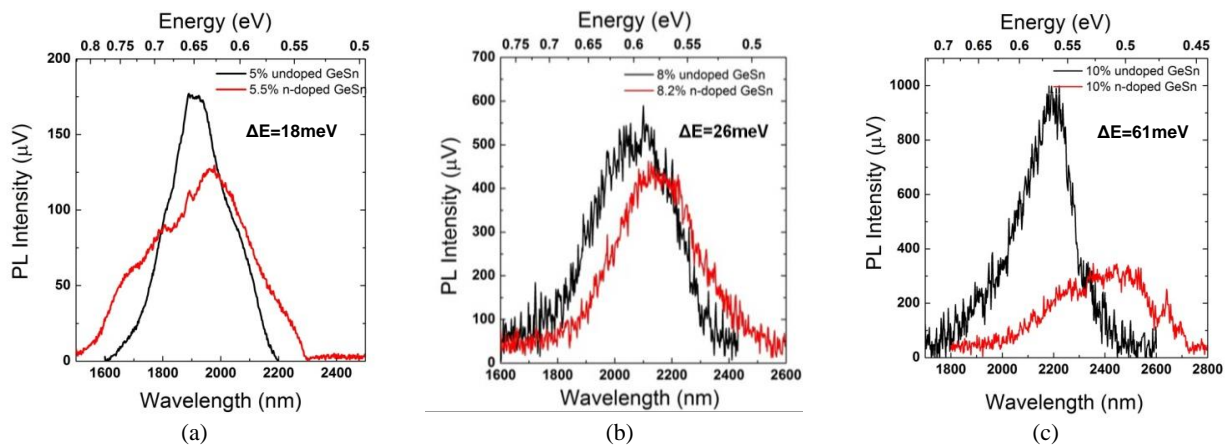


Fig. 17. Comparison of PL spectra between unintentionally doped and heavily doped n-type GeSn samples with Sn composition of (a) 5%, (b) 8% and (c) 10%. The bandgap shrinkage due to high doping is observed.

Fig. 17 (a)-(c) show the PL spectra of n-type doped GeSn samples and their comparison with unintentionally doped samples with similar Sn composition. The doping level for samples with Sn compositions of 5.5, 8.2, and 10% are 6.5×10^{19} , 1×10^{19} , and $0.3 \times 10^{19} / \text{cm}^{-3}$, respectively. Comparing with the unintentionally doped samples, the bandgap shrinkage due to the n-type doping is observed as 18, 26,

and 61meV for 5.5, 8.2, and 10% Sn samples, respectively. While the result is expected, this is first time observed in GeSn material system.

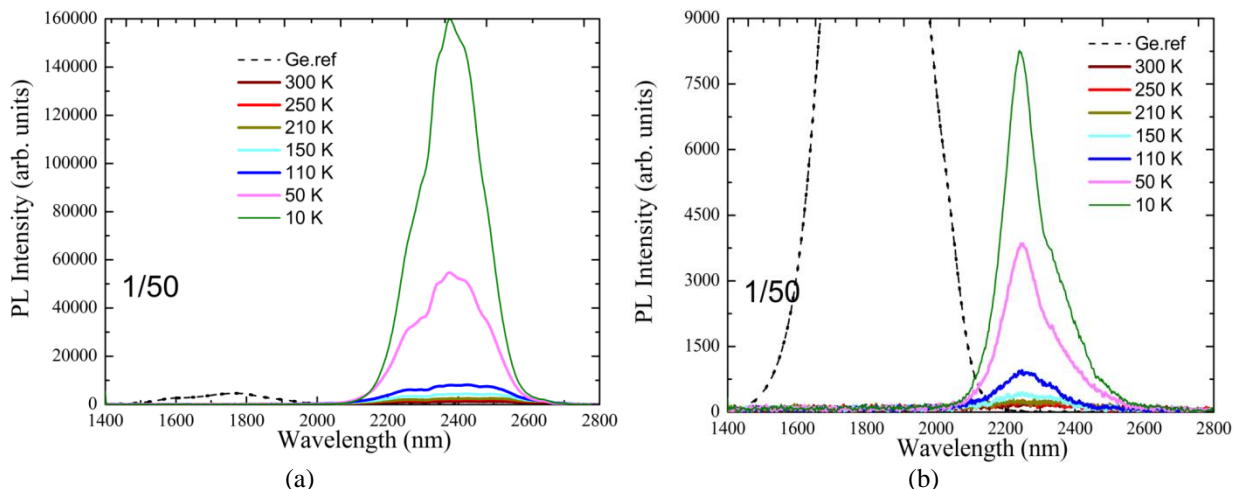


Fig. 18. Temperature dependent PL of n-type doped (a) 10% Sn (b) 11% Sn samples.

Figure 18 shows temperature dependent PL spectra of 10 and 11% n-type doped GeSn samples. As temperature decreases, the PL intensity dramatically increases, indicating these samples are direct bandgap materials. The optically pumped lasing might be expected from these samples. More experiments are underway.

III. Development of high performance GeSn mid-IR detectors and emitters

GeSn samples have been fabricated into photoconductive detectors, avalanche photo diodes (APDs), and light-emitting diodes (LEDs). Characterization of these devices has been conducted.

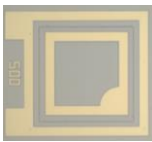
i) High performance GeSn photodetectors

By leveraging the high quality GeSn material growth capability, the team has developed a set of processes for different photo detectors. In-depth of study has been conducted for GeSn photo conductors and preliminary study has been done for GeSn photodiodes and avalanche photodiodes (APDs). A summary of the photo detector work is given in Table IV and the significant results are given in below.

- Spectral photo response of photoconductors with Sn compositions up to 10% has been investigated with longwave cutoff extended to 2.4 μm ;
- Temperature-dependent characterization of photoconductors has been conducted and the increased responsivity and specific detectivity (D^*) with decreased temperature has been observed;
- The responsivity of 1.63 A/W at 1.55 μm has been achieved with a $\text{Ge}_{0.9}\text{Sn}_{0.1}$ standard photoconductor at 77 K, which is higher than that of market dominating Ge (0.8 A/W) and standard InGaAs (1.05 A/W) detectors at the same wavelength;
- A side by side comparison for D^* between GeSn and other market dominating IR detectors in short-IR wavelength. This is the first time reported D^* of a GeSn detector as a function of wavelength;
- A newly designed photoconductor with interdigitated electrodes has been fabricated and characterized. Due to the reduced carrier transit time, a high gain is achieved. As a result, a measured responsivity of 2.85 A/W at 77 K has been obtained at 1.55 μm .



Table IV Summary of photo detector devices

Type of photo detector	Top view of device image	Sn composition	Specifications
Standard Photoconductor		1-10%	<ul style="list-style-type: none"> GeSn bulk samples; For baseline study of photo response, carrier lifetime and material quality evaluation.
Interdigitated photoconductor		1-10%	<ul style="list-style-type: none"> GeSn bulk samples; Newly designed high gain photoconductor; Interdigitated electrodes with spacing of 6, 12, and 24 μm; Effective carrier lifetime evaluation; Capability of high speed operating measurement.
Photo diode		6, 8, 9, 10%	<ul style="list-style-type: none"> Ge/GeSn/Ge n-i-p DHS; Low dark current; Low voltage operation.
Avalanche photo diode		0 (Ge), 7%	<ul style="list-style-type: none"> GeSn/Si Separate SACM structure; Taking advantage of excellent optical absorption of GeSn and the outstanding carrier multiplication properties of Si.

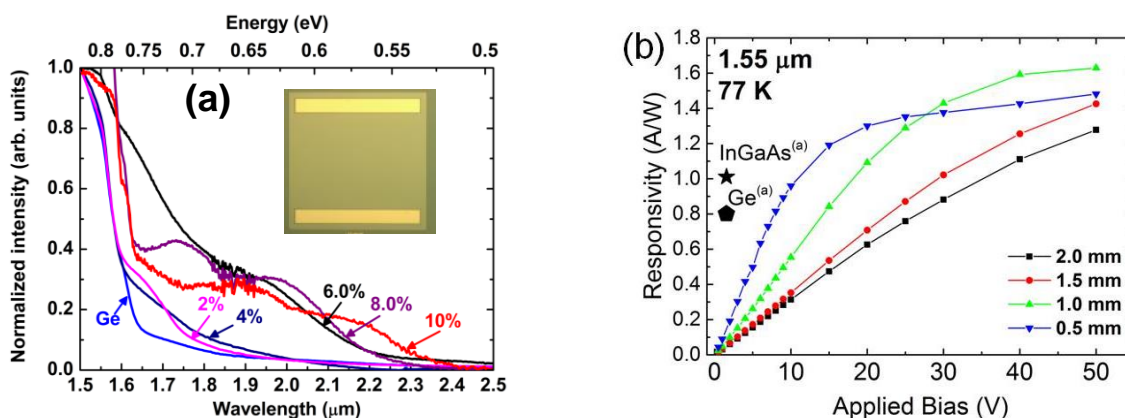


Fig. 19. (a) Room temperature spectral photo response of standard photoconductors with Sn compositions up to 10 %. (b) Responsivity measured at 77 K for each mesa size of Ge_{0.9}Sn_{0.1} photoconductor. Representative responsivities of InGaAs and Ge detectors are given for comparison.

Photoconductors: Room temperature spectral photo response of standard photoconductors has been measured as shown in Fig. 19(a). As Sn composition increases, the cutoff wavelength shifts towards to longer wavelength and the longest cutoff wavelength of 2.4 μm is observed for a 10 % Sn device. Temperature dependent responsivity for different device sizes and bias voltages are conducted thoroughly. Typical Ge_{0.9}Sn_{0.1} photoconductor responsivity result measured at 1.55 μm under 77 K is shown in Fig. 19(b). The saturation of the responsivity is due to the carrier sweep-out effect. The peak responsivity value of 1.63 A/W measured at 77 K, was observed at 50 V bias on a 1 mm mesa device. At 77 K, the



responsivity of $\text{Ge}_{0.9}\text{Sn}_{0.1}$ photoconductors exceeds that of commercially available InGaAs and Ge photovoltaic detectors at 1.55 μm .

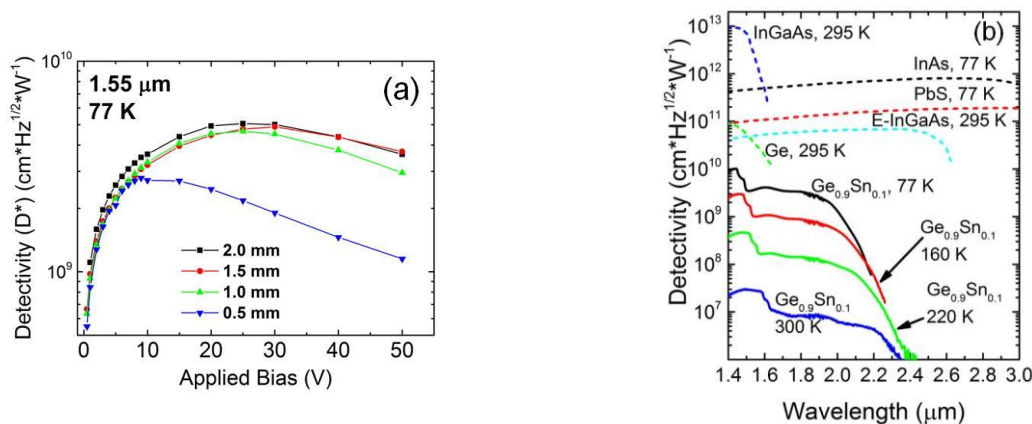


Fig. 20. (a) D^* measured for 77 K at a 1.55 μm wavelength. Measurements were conducted on each mesa size as a function of the applied voltage bias. (b) D^* for 300, 220, 160, and 77 K were measured with a 10 volt DC bias across the 2.0 mm mesa device. D^* for other detectors in the same spectral range are plotted for comparison.

Using the 1 Hz equivalent noise bandwidth of the measurement setup, the known device area, and the calculated noise current, the D^* in Fig. 20(a) is calculated based on the measured AC responsivity values from Fig. 19(b). The responsivity saturates at high voltage, while the noise component increases as $V^{1/2}$ leading to the overall decreasing D^* for further increased bias. The peak D^* value $5 \times 10^9 \text{ cm}^2\text{Hz}^{1/2}\text{W}^{-1}$ of the 2.0 mm detector occurs at an applied bias of 25 V, followed by a decrease in D^* for further increasing bias. The spectral D^* in Fig. 20(b) for different temperatures shows the comparison of these devices with other mature detector technologies. Note that the D^* of $\text{Ge}_{0.9}\text{Sn}_{0.1}$ is only one order-of-magnitude lower than that of Ge, extended-InGaAs, and PbS detectors in the short wavelength IR range. A reduction of the device dark current through thicker active layers and a decrease of the dominant noise by reducing defects at the growth interface would dramatically improve the D^* for these types of $\text{Ge}_{1-x}\text{Sn}_x$ detectors, making their performance superior to the commercially available IR detectors in the same wavelength range.

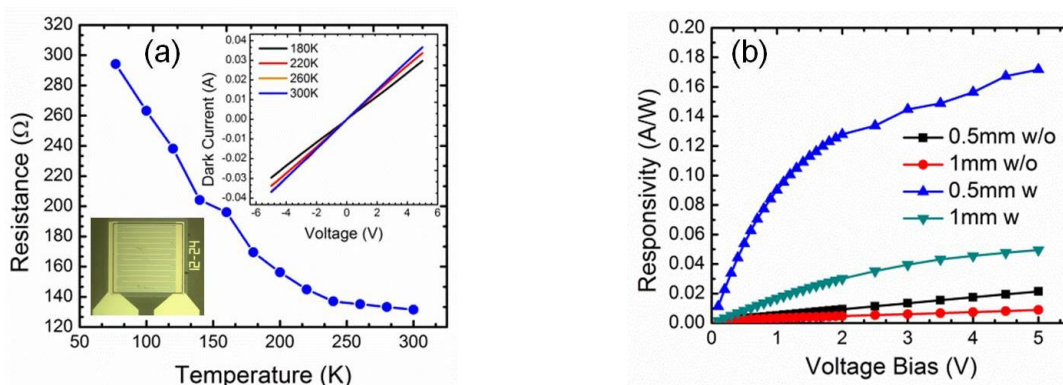


Fig. 21. (a) The dark resistance of the 0.5 mm mesa device. Insets: Optical image top view of the device and linear behavior of dark I-V indicates good Ohmic contact. (b) Comparison of responsivities between the devices with and without interdigitated electrodes.

Photoconductor with interdigitated electrodes: In order to obtain a high gain photoconductor, a newly designed photoconductor with interdigitated electrodes has been fabricated and characterized. Figure 21(a) plots the resistance value extracted from the dark I-V measurement at temperatures from 300 to 77

K. The linear I-V shown in the inset indicates good Ohmic contact. As the temperature decreases, the resistance increases as a result of the decreasing number of activated carriers in the device. The responsivities of the Ge_{0.9}Sn_{0.1} photoconductor with and without interdigitated electrodes at room temperature are shown in Fig. 21(b). The newly designed interdigitated photoconductor allows an enhancement factor of 8 for the 0.5 mm mesa device and 5.6 for the 1 mm mesa device under 5 V bias, respectively.

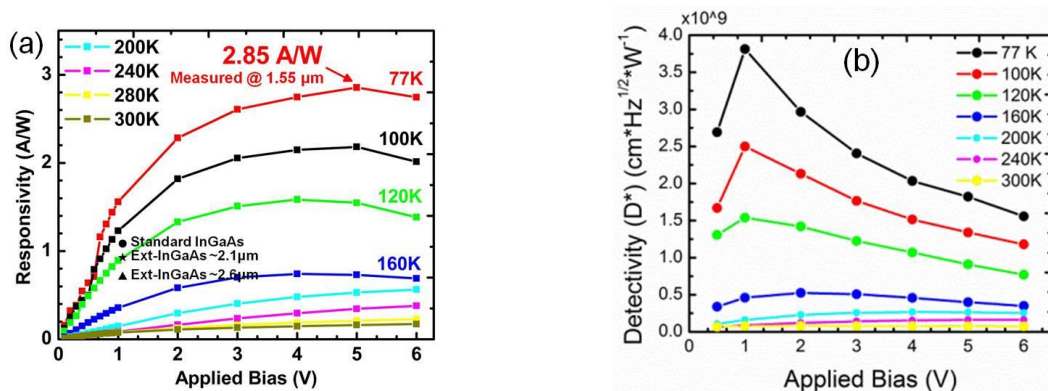


Fig. 22. (a) Responsivity measured for the 0.5 mm mesa device at temperatures from 300 to 77 K. Responsivities for other detectors at 1.55 μm are plotted for comparison. (b) D* of the 0.5 mm mesa device at temperatures from 300 to 77 K.

Figure 22(a) shows a clear enhancement of responsivity with decreasing temperature for the 0.5 mm mesa device. A maximum responsivity of 2.85 A/W under 5 V bias at 77 K was achieved, which is three times of commercially available InGaAs and Ge photovoltaic detectors at 1.55 μm. As temperature decreases, the activated background carrier concentration is reduced while the effective carrier lifetime increases, resulting in the improvement of the responsivity at low temperature. The D* was consequently calculated based on measured responsivity at different temperatures, as shown in Fig. 22(b). For this set of devices wherein the dark current is high, the shot noise dominates over other noise mechanisms. As applied voltage increases, the noise current increases proportionally with V^{1/2} while the responsivity saturates. Therefore the D* decreases after a certain applied voltage. At 77 K, the peak D* value of 3.81x10⁹ cm*Hz^{1/2}*W⁻¹ was observed at 1 V. The D* can be improved by optimizing the geometry parameters of interdigitated electrodes to allow high responsivity and low noise current.

Photodiodes: The team has developed GeSn photodiode detector, which is a more commonly used photodetector architecture. The Ge/GeSn/Ge NIP (double heterostructure) DHS samples were fabricated into photodiodes. The electrical and optical characterization including temperature dependent I-V, spectrum response, and noise measurement have been conducted.

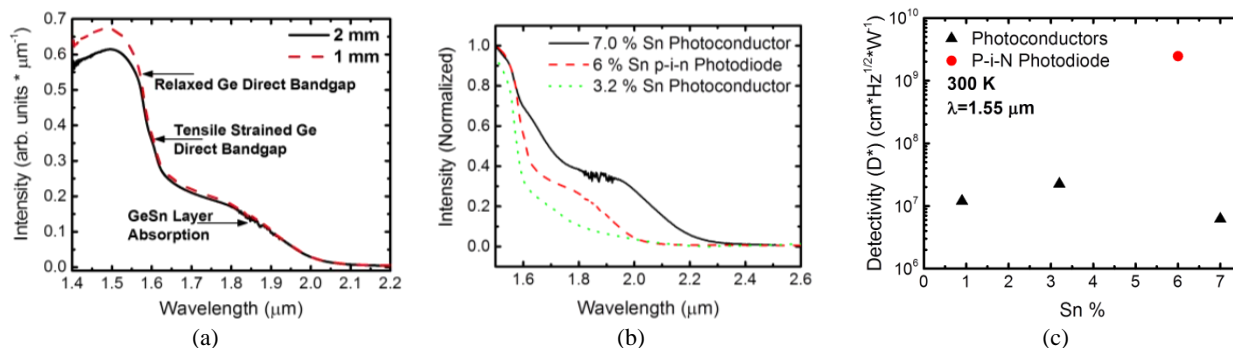


Fig. 23. (a) Spectral response of the 6 % Sn p-i-n photodiodes with 1 and 2 mm mesa sizes. (b) Spectral response of 6% Sn photo diode compared with 3.2 and 7.0 % Sn photoconductors. (c) D* of 6% Sn photo diode detector. The D* of photoconductor is



plotted for comparison.

As shown in Fig. 23(a) and (b), photo response up to 2 μm has been observed for a 6 % GeSn photo diode and the response was compared with two different photoconductors (3.2 and 7% Sn). Since our GeSn photodiode has much lower dark current (at reverse applied voltage) compared to photoconductor, the D^* of photo diode is two order of magnitude higher than that of photoconductor, as shown in Fig. 23(c). The preliminary result shows great promises of GeSn photodiode to achieve high performance.

APD: Avalanche photo diode based on Separate Absorption-Charge-Multiplication (SACM) structure has been grown by ASM. The design (shown in Fig. 24(a)) takes advantage of the excellent optical absorption of GeSn at mid-IR range and the outstanding carrier multiplication properties of Si. In the high-electric-field gain region of Si, photogenerated electrons from the GeSn absorption layer undergo a series of impact ionization processes, which consequently amplifies the photocurrent and improves the sensitivity. Figure 24(b) shows a schematic of the cross-section for the APD device. Due to the current growth limitation, GeSn layer (7% Sn) was grown on a thick Ge buffer layer not directly on Si. The preliminary testing results of the temperature dependent I-V curves have shown device breakdown behavior in Fig. 24(c). However, the device spectrum response does not show any IR response due to GeSn or Ge absorption. It is believed that the conduction band discontinuity might be the reason to stop electron propagating to Si for avalanche process. A possible solution is to engineer the local doping profile so that the electron could be easily collected. More through characterizations will be conducted and new generation of devices will be designed and fabricated.

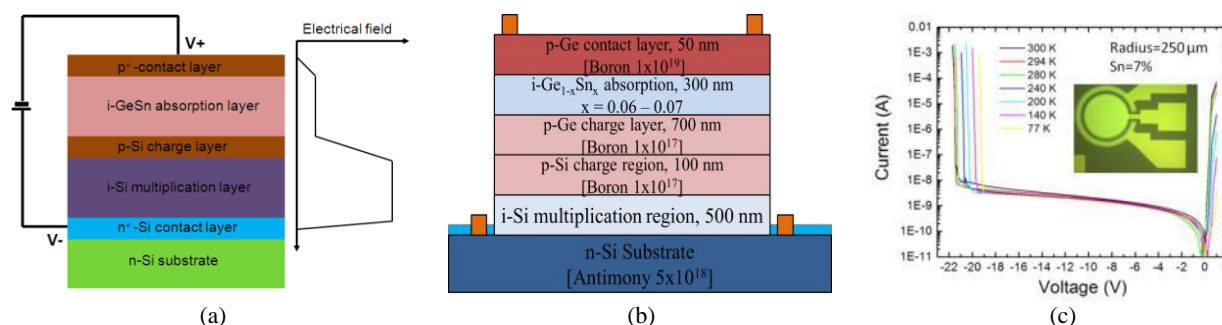
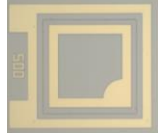


Fig. 24 (a) Schematic cross-section of a GeSn/Si APD with a SACM structure and its internal electric field distribution. (b) Structure of GeSn avalanche photo diode (APD) with a SACM structure. (c) Temperature dependent I-V of 7% Sn APD indicates the breakdown voltage. Inset: Optical image of the device.

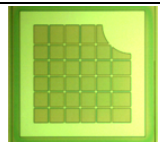
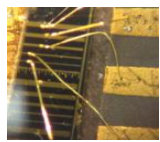
ii) High performance GeSn emitters

On the basis of the existing Ge/GeSn/Ge DHS samples, both proof-of-concept and high power surface emitting LEDs were fabricated. In addition, the samples were also fabricated to edge-emitting devices and the similar process is intended to be used for future laser fabrication. Table V lists the research summary of GeSn LED and the significant results are listed below.

Table V Summary of GeSn based LED

Type of LED device		Top view of device image	Sn compositions: 6, 8, 9, 10%
			Specifications
Surface emitting LED	1 st generation		<ul style="list-style-type: none"> • For baseline study, material quality evaluation; • Device sizes from 0.5 to 2mm in side length.



	2 nd generation		<ul style="list-style-type: none"> • For in-depth study. Extended metal pads for wire bonding; • High power emission; • Device sizes from 50 to 250μm in radius.
	3 rd generation		<ul style="list-style-type: none"> • Fishnet top contact design for uniform current flow; • High power emission; • Device sizes from 0.5 to 2mm in side length.
	Edge emitting LED		<ul style="list-style-type: none"> • Pioneer study of group IV based electrical injection laser; • Light source for On-chip integration sensing system applications; • Device sizes from 80 to 120μm in cavity width, and 500~800 μm in cavity length.

- Room temperature EL spectra of the 1st generation LEDs with Sn compositions from 6 to 10% have been investigated. The red-shift of EL peak with higher Sn composition has been observed. The peak power is ~28 mW for a 10% Sn LED;
- Temperature-dependent EL emissions from the 2nd generation LEDs with Sn compositions of 6 and 8% have been investigated. The blue-shift of EL peak with decreased temperature has been observed. A peak power of 0.1 W was measured for a 8% Sn LED;
- Edge emitting LEDs have been fabricated and characterized. The EL spectra agree well with surface emitting LED at same Sn composition. A peak power of 50 mW has been achieved for a 8% Sn LED;
- Temperature-dependent EL emissions from edge emitting LEDs with Sn composition of 8% have been measured.

1st generation LED: Fig. 25(a) shows the normalized EL spectra for 1st generation surface emitting LEDs at room temperature. As Sn composition increases, the EL peak position shifts to longer wavelength. The EL emission at 2380 nm was observed from 10% Sn LED. For the devices with 9 and 10% Sn LEDs the PbS detector (cut-off at 3 μ m) is applied to measure the spectra, whose signal-to-noise ratio is lower than that of the InGaAs detector (cut-off at 2.3 μ m) which is used to measure the EL of LEDs with 6 and 8% Sn LEDs.

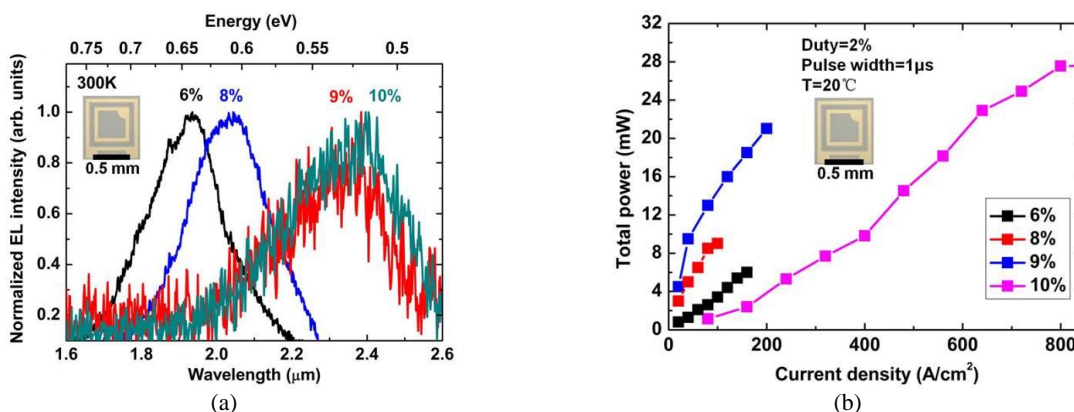


Fig. 25. (a) Normalized EL spectra of 1st generation LEDs at 300 K. (b) The peak emission power of 6, 8, 9, and 10% Sn LED at 20 °C.

The emission power measurement has been performed by using a pulsed current source in order to eliminate the contribution from Joule heating. Figure 25 (b) shows the peak emission power for 6, 8, 9



and 10% Sn 1st generation LEDs (0.5 mm square mesa device) at 20 °C. With a 2% duty cycle and 1 μs pulse width of current source, the maximum peak power of ~28 mW at 800 A/cm² has been obtained from a 10% Sn LED.

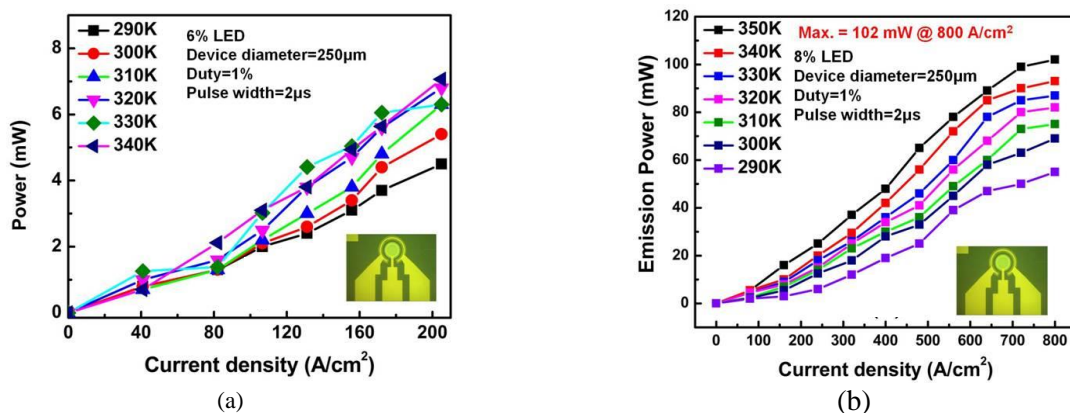


Fig. 26. The peak emission power of (a) 6% Sn and (b) 8% Sn 2nd generation LED under different current injection at temperatures from 290 to 340 K.

2nd generation LED: The 2nd LEDs show similar Sn composition dependent spectra behavior. Temperature-dependent power measurement has been conducted for 6 and 8% Sn LEDs with 250 μm in device diameter from 290 to 350 K, as shown in Fig. 26. Current with 1% duty cycle and 2 μs pulse width was applied. As temperature increases, the peak emission power increases under the same current injection level. This is due to the more injected carriers populate the Γ valley with increased temperature; therefore the radiative recombination was enhanced, resulting in the increased emission power. The peak emission power of 0.1 W has been achieved for a 8% Sn LED at an injection of 800 A/cm² and a working temperature of 350 K, as shown in Fig. 26(b).

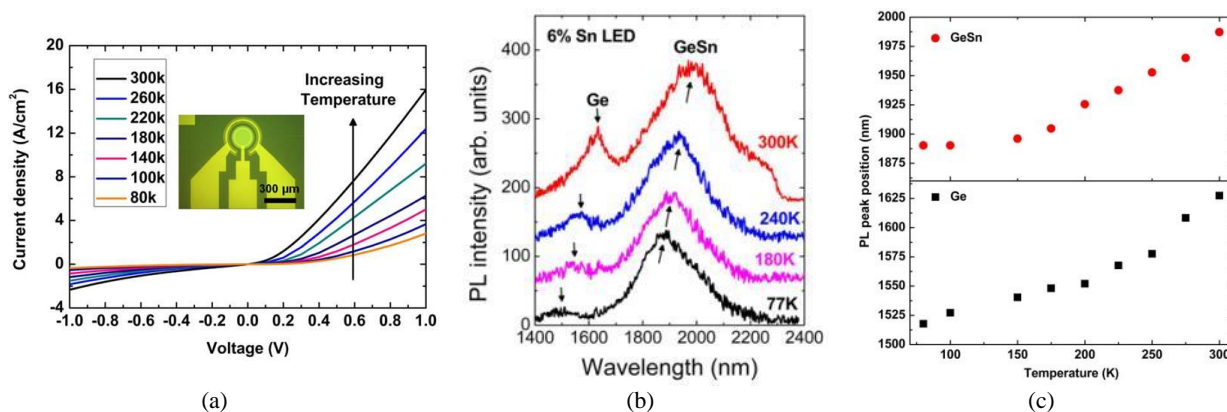


Fig. 27. Characteristics of 2nd generation 6% Sn LED. (a) The temperature-dependent I-V characteristic. Inset: Optical image top view image of the device. (b) The temperature-dependent EL emission spectra (c) Peak position as function of temperature extracted from (b).

The temperature-dependent behaviors of 2nd generation Ge_{0.94}Sn_{0.06} LEDs have been investigated at temperatures from 80 to 300 K. The current-voltage characteristic and optical image top view of the device are shown in Fig. 27(a). The clearly rectifying behavior is observed at temperatures from 80 to 300 K. The decrease in device resistance by increasing the temperature is due to the increasing number of activated carriers in the device. Figure 27(b) shows the temperature-dependent EL spectra of Ge_{0.94}Sn_{0.06} LED from 80 to 300 K at an injection level of 600 A/cm². The peak shift to shorter wavelength at lower temperature is observed, which is consistent well with Varshni's relation: $E_g(T) = E_g(0) - \frac{\alpha T^2}{T + \beta}$, where

$E_g(0)$ is the bandgap energy of $\text{Ge}_{0.94}\text{Sn}_{0.06}$ at zero K, T is temperature, and α and β are fitting parameters. Based on the $E_g(0) = 0.63 \text{ eV}$ and the peak position varying from 1980 nm at 300 K to 1900 nm at 80 K, the α and β are fitted as $3.2 \times 10^{-4} \text{ eV/K}$ and 275 K, respectively, which agrees with previous study on temperature-dependent PL spectra of 6% Sn sample. A small peak at around 1550 nm in most EL spectra is attributed to EL from the Ge layer, whose direct bandgap energy is 0.8 eV at room temperature. The EL peak position as function of temperature is summarized in Fig. 27(c).

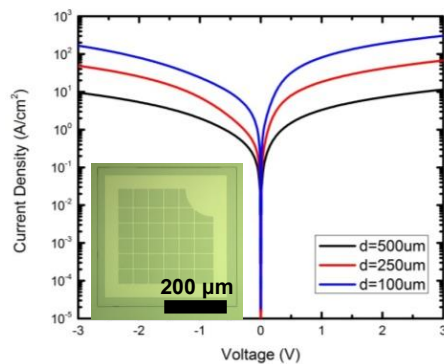


Fig. 28. Current-voltage curves of 10% Sn 3rd generation LED with fishnet top contact structures.

3rd generation LED: For the 3rd generation LED, the fishnet structure is used for top contact in order to improve the uniformity of current injection. Moreover, the high power emission can be expected with larger active area of emitter. The preliminary current-voltage results are shown in Fig. 28. Detailed characterization is underway.

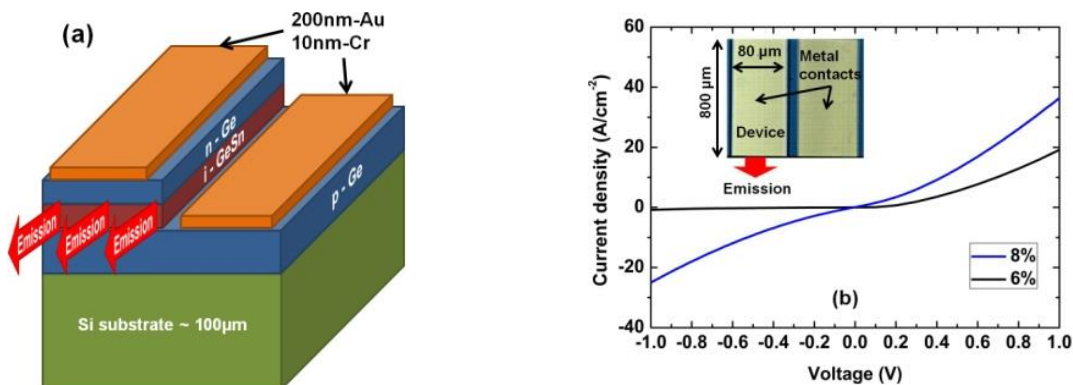


Fig. 29. (a) Schematic of the device; (b) I-V characteristics. The inset shows top view image of the device.

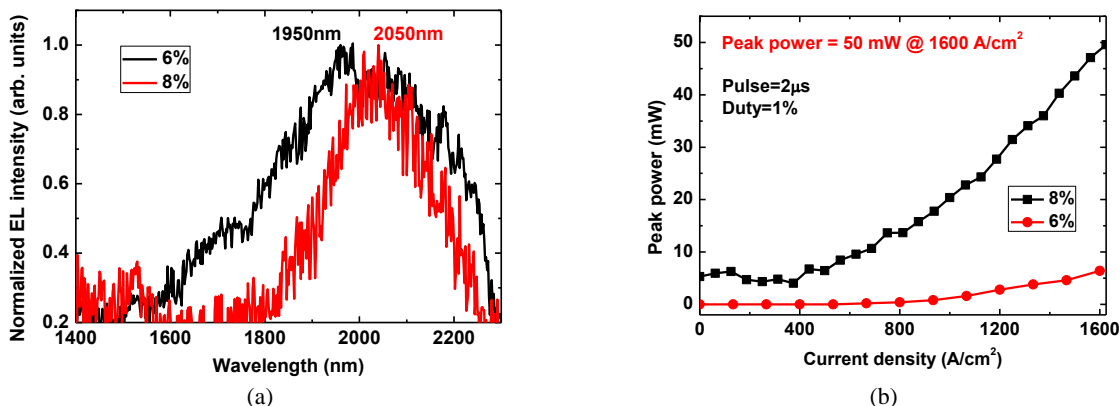


Fig. 30. (a) Room temperature EL spectra of 6 and 8% Sn edge emitting LEDs; (b) Peak emission powers of 6 and 8% Sn LEDs at room temperature.



Edge emitting LED: The samples were also fabricated to edge-emitting devices. Figure 29(a) shows the schematic drawing of the device. The current-voltage characteristic and optical image top view of the device are shown in Fig. 29(b) ($W=80\ \mu\text{m}$, $L=800\ \mu\text{m}$). The clearly rectifying behavior is observed, indicating the good Ohmic contact. As Sn composition increases, the current density increases under the same forward voltage due to the narrowed bandgap with higher Sn composition.

Figure 30(a) shows normalized EL spectra of 6 and 8% Sn LEDs at room temperature. As the Sn composition increases, the EL peak shifts towards longer wavelength due to the reduced bandgap energies. The EL emission at 1950 and 2050 nm were observed from 6 and 8% Sn LEDs, respectively. These results are consistent with surface emitting LEDs. Figure 30(b) shows the peak emission power as a function of current injection densities at room temperature. For each LED, the emission power increases as current increases. A saturation power was observed at $1600\ \text{A}/\text{cm}^2$, which is due to the voltage compliance of the current source. As Sn composition increases, the peak power increases under the same current injection. The peak emission power of 50 mW has been achieved for a 8% Sn edge emitting LED at an injection of $1600\ \text{A}/\text{cm}^2$.

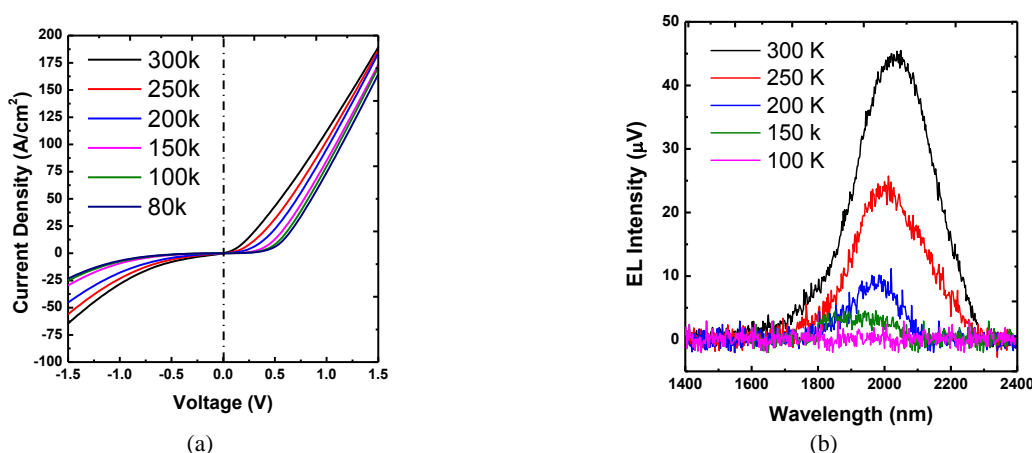


Fig. 31. Temperature dependent (a) current voltage and (b) EL spectra of 8% Sn edge emitting LED.

The temperature-dependent behaviors of edge emitting $\text{Ge}_{0.92}\text{Sn}_{0.08}$ LED have been investigated at temperatures from 80 to 300 K. The current-voltage characteristic and optical image top view of the device are shown in Fig. 31(a). The clearly rectifying behavior is observed at temperatures from 80 to 300 K. Figure 31(b) shows the temperature-dependent EL spectra of $\text{Ge}_{0.92}\text{Sn}_{0.08}$ LED from 80 to 300 K at an injection level of $600\ \text{A}/\text{cm}^2$. The peak shift to shorter wavelength at lower temperature is observed, which is consistent well with Varshni's relation.

iii) Optically pumped GeSn lasers

The team has built an optical pumping setup in order to study the GeSn lasing characteristics. Since the recent demonstration of GeSn lasers were conducted on a F-P cavity structure pumped with a Nd:YAG pulsed laser, we adopted a similar approach while using the fs Ti:Sapphire laser which could provide sufficiently high pumping power. The mirrors of the F-P cavity was formed by lapping the Si substrates and then cleaving of end facets. Figure 32(a) shows the schematic of the optical pumping F-P cavity experiment with pumping light collimated to a narrow stripe using a cylindrical lens. As temperature decreases, the PL intensity dramatically increases and the peak becomes symmetric as shown in Fig. 32(b), indicating the lasing can be expected at lower temperature with improved light confinement. More experiments are underway.



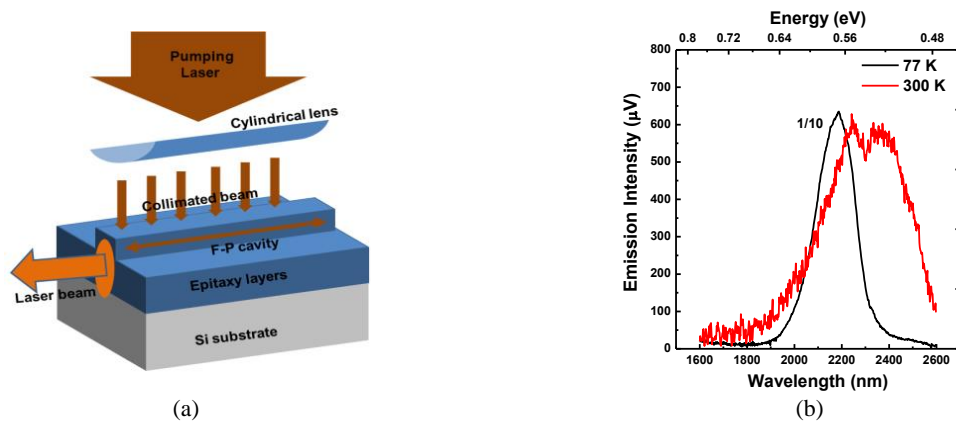


Fig. 32. (a) Schematic of the optical pumping experiment for an F-P laser. (b) Edge emitting PL spectra of 10% Sn n-type doped sample at 77 and 300 K.

IV. Others

Kick-off meeting

- A kick-off meeting was held on July 17th, 2014 at AFOSR. Prof. Shui-Qing (Fisher) Yu on behalf of Arktonics, LLC attended the meeting and had a fruitful discussion with the program manager Dr. Gernot Pomrenke.

Highlights

- The GeSn detector work from Yu's group published in early this year was reported by several media including *Laser Focus World* and *Science Daily* to show the visibility of GeSn material and devices to the community. While this work is not directly related to this project, Arktonics was mentioned in the report as a collaborator for future commercialization. We are confident that the outcome from this SBIR project will achieve the same level of publicity. Several links for the report are given in below:

<http://www.pddnet.com/news/2014/09/germanium-tin-cheaper-smartphones>

<http://phys.org/news/2014-09-germanium-tin-cheaper-infrared-cameras.html>

<http://www.azom.com/news.aspx?newsID=42434>

<http://www.newswise.com/articles/germanium-tin-could-mean-better-and-cheaper-infrared-cameras-in-smartphones>

<http://www.laserfocusworld.com/articles/2014/09/cmos-compatible-germanium-tin-on-silicon-could-make-inexpensive-ir-camera-sensor.html>

http://www.opli.net/opli_magazine/eo/2014/germanium-tin-could-mean-better-and-cheaper-infrared-cameras-in-smartphones-sept-news/

<http://www.sciencedaily.com/releases/2014/09/140918121338.htm>

- The paper "Shortwave-infrared photoluminescence from $\text{Ge}_{1-x}\text{Sn}_x$ thin films on silicon" published in *Journal of Vacuum Science & Technology B* was selected as Featured Letters.
- The paper "Competition of optical transitions between direct and indirect bandgaps in $\text{Ge}_{1-x}\text{Sn}_x$ " published in *Applied Physics Letters* was highlighted for the latest research in thin film by AIP.

Facilities update

- A new continuous wave laser (operating at 532nm) with maximum power of 500 mW has been installed and used for GeSn optical characterization.



- A new spectrometer (Not funded by this project) has been installed in a standalone EL measurement system. The low temperature and pulsed EL measurement with a high injection up to 3 A has been performed (see LED characterization results).
- A low temperature optical pumping setup for edge-emitting lasers using a fs Ti:Sapphire laser was constructed and the initial testing result was obtained and reported (see optically pumped GeSn laser results)
- Arktonics, LLC has full access to these UA research facilities through agreement with UA as an external user.

V. Publications

Journal papers

Published:

- [1] Wei Du, Seyed A. Ghetmiri, Benjamin R. Conley, Aboozar Mosleh, Amjad Nazzal, Richard A. Soref, Greg Sun, John Tolle, Joe Margetis, Hameed A. Naseem, and Shui-Qing Yu, "Competition of optical transitions between direct and indirect bandgaps in $\text{Ge}_{1-x}\text{Sn}_x$," *Applied Physics Letters*, **105**, 051104 (2014).
- [2] Seyed Amir Ghetmiri, Wei Du, Benjamin R. Conley, Aboozar Mosleh, Amjad Nazzal, Richard A. Soref, Greg Sun, Joe Margetis, John Tolle, Hameed A. Naseem, and Shui-Qing Yu, "Shortwave-infrared photoluminescence from $\text{Ge}_{1-x}\text{Sn}_x$ thin films on silicon", *Journal of Vacuum Science & Technology B*, **32**, 060601 (2014).
- [3] Seyed Amir Ghetmiri, Wei Du, Joe Margetis, Aboozar Mosleh, Larry Cousar, Benjamin R. Conley, Lucas Domulevicz, Amjad Nazzal, Greg Sun, Richard A. Soref, John Tolle, Baohua Li, Hameed A. Naseem, and Shui-Qing Yu, "Direct-bandgap GeSn grown on Silicon with 2230 nm photoluminescence", *Applied Physics Letters*, **105**, 151109 (2014).
- [4] Benjamin R. Conley, Joe Margetis, Wei Du, Huong Tran, Aboozar Mosleh, Seyed Amir Ghetmiri, John Tolle, Greg Sun, Richard Soref, Baohua Li, Hameed A. Naseem, and Shui-Qing Yu, "Si based GeSn photoconductors with a 1.63A/W peak responsivity and a 2.4 μm longwavelength cutoff", *Applied Physics Letters*, **105**, 221117 (2014).

Accepted/Submitted:

- [5] Aboozar Mosleh, Murtadha Alher, Larry C. Cousar, Wei Du, Seyed Amir Ghetmiri, Thach Pham, Benjamin R. Conley, Joshua M. Grant, Greg Sun, Richard A. Soref, Baohua Li, Hameed A. Naseem, Shui-Qing Yu, "Direct growth of $\text{Ge}_{1-x}\text{Sn}_x$ films on Si using a cold-wall ultra-high-vacuum chemical-vapor-deposition system", Initially submitted to *Journal of Crystal Growth* in 2014, now **Accepted** for publication by *Frontiers in Materials* (2015).
- [6] T. N. Pham, W. Du, B. R. Conley, J. Margetis, G. Sun, R. A. Soref, J. Tolle, B. Li and S. -Q. Yu, "Si based $\text{Ge}_{0.9}\text{Sn}_{0.1}$ photo detector with a peak responsivity of 2.85 A/W and a longwave cutoff at 2.4 μm ", **Accepted** for publication by *Electronics Letters* (2015).

Conference contributions

Published:

- [1] Shui-Qing Yu, Wei Du, Benjamin R. Conley, Seyed A. Ghetmiri, Aboozar Mosleh, Thach Pham, Yiyin Zhou, Amjad Nazzal, Greg Sun, Richard A. Soref, Joe Margetis, John Tolle, Baohua Li, and Hameed A. Naseem, "GeSn Photodetector and Light Emitter: Mid-Infrared Devices in Silicon Photonics", **Invited talk**, *SPIE Photonic West*, February 7~12, San Francisco, CA (2015).
- [2] Benjamin R. Conley, Wei Du, Richard A. Soref, Greg Sun, Joe Margetis, John Tolle, Baohua Li, Shui-Qing Yu, "Enhanced gain of GeSn photoconductors by interdigitated electrodes for mid-infrared detection", **Oral presentation**, *SPIE Photonic West*, February 7~12, San Francisco, CA (2015).



- [3] S.-Q. Yu, S. A. Ghetmiri, W. Du, J. Margetis, Y. Zhou, A. Mosleh, S. Al-Kabi, A. Nazzal, G. Sun, R.A. Soref, J. Tolle, B. Li, H.A. Naseem, "Si based GeSn light emitter: mid-infrared device in Si photonics", Proceedings of SPIE, vol. **9367**, Silicon Photonics X, 93670R, (February 27 2015).
- [4] Thach Pham, Wei Du, Joe Margetis, Seyed Amir Ghetmiri, Aboozar Mosleh, Greg Sun, Richard A Soref, John Tolle, Hameed A. Naseem, Baohua Li, and Shui-Qing Yu, "Temperature-dependent study of Si-based GeSn photoconductors", Proceedings of SPIE, vol. **9367**, Silicon Photonics X, 93670S, (February 27, 2015).

Accepted/Submitted:

- [5] Shui-Qing Yu, Wei Du, Benjamin R. Conley, Seyed A. Ghetmiri, Aboozar Mosleh, Thach Pham, Yiyin Zhou, Amjad Nazzal, Greg Sun, Richard A. Soref, Joe Margetis, John Tolle, Baohua Li, and Hameed A. Naseem, "Si based mid-infrared GeSn photo detectors and light emitters on silicon substrates", **Invited talk**, *SPIE Optics + Photonics*, August 9~13, San Diego, CA (2015).
- [6] Seyed Amir Ghetmiri, Wei Du, Yiyin Zhou, Joe Margetis, Thach Pham, Aboozar Mosleh, Benjamin R. Conley, Greg Sun, Richard Soref, John Tolle, Hameed A. Naseem, Baohua Li, Shui-Qing Yu, "Temperature-dependent characterization of Ge_{0.94}Sn_{0.06} Light Emitting Diode grown on Si via CVD", **Accepted as oral presentation**, *the Conference On Lasers and Electrooptics (CLEO) 2015*, ATu1J.6, May 10~15, San Jose, CA (2015).
- [7] Thach Pham, Benjamin R. Conley, Joe Margetis, Huong Tran, Seyed Amir Ghetmiri, Aboozar Mosleh, Wei Du, Greg Sun, Richard A Soref, John Tolle, Hameed A. Naseem, Baohua Li, and Shui-Qing Yu, "Enhanced responsivity up to 2.85 A/W of Si-based Ge_{0.9}Sn_{0.1} photoconductors by integration of interdigitated electrodes", **Accepted as oral presentation**, *the Conference On Lasers and Electrooptics (CLEO) 2015*, STh1I.7, May 10~15, San Jose, CA (2015).
- [8] Wei Du, Seyed A. Ghetmiri, Yiyin Zhou, Aboozar Mosleh, Joe Margetis, John Tolle, Greg Sun, Richard A. Soref, Baohua Li, Hameed Naseem, and Shui-Qing Yu, "Si-Based GeSn Edge-Emitting LEDs with Sn Compositions up to 8%", **Submitted to 2015 IEEE Summer Topicals**.
- [9] Aboozar Mosleh, Murtadha Alher, Wei Du, Larry C. Cousar, Seyed Amir Ghetmiri, Sattar Al-Kabi, Wei Dou, Perry C. Grant, Benjamin R. Conley, Greg Sun, Richard A. Soref, Baohua Li, Hameed A. Naseem, and Shui-Qing Yu, "Growth and characterization of buffer-free SiGeSn epitaxial layers on Si for photonic applications", **Accepted as oral presentation by 2015 Electronic Material Conference**.
- [10] Sattar Al-Kabi, Seyed Amir Ghetmiri, Wei Du, Huong Tran, Greg Sun, Richard Soref, John Tolle, Joe Margetis, Baohua Li, Hameed A. Naseem, and Shui-Qing Yu, "Material and Optical Characterizations for Both Bulk and NIP Double Heterostructure of Germanium Tin", **Accepted as poster presentation by 2015 Electronic Material Conference**.

VI. Cumulative list of people involved in this AF SBIR Phase I

Baohua Li (President, Arktonics, LLC, P. R. China, U.S. permanent resident, PI)
Larry Cousar (Research engineer, Arktonics, LLC, U. S.)
Husam Abu-Safe (Research engineer, Arktonics, LLC, U. S.)
John Tolle (U. S., Consultant)
Radek Roucka (Czech Republic, U.S. permanent resident, Consultant)
Shuiqing Yu (Associate professor, University of Arkansas, P. R. China, U.S. permanent resident, PI of the subcontractor)
Wei Du (Postdoctoral research associate, University of Arkansas, P. R. China, J1 visa)
Benjamin R. Conley (Graduate student, University of Arkansas, U.S.)
Seyed Amir Ghetmiri (Graduate student, University of Arkansas, Iran, F1 visa)
Yiyin Zhou (Graduate student, University of Arkansas, P. R. China, F1 visa)
Perry Grant (Graduate student, University of Arkansas, U.S.)



Wei Dou (Graduate student, University of Arkansas, P.R. China, F1 visa)
Aboozar Mosleh (Graduate student, University of Arkansas, Iran, F1 visa)



Publications:

Journal papers

- [1] Wei Du, Seyed A. Ghetmiri, Benjamin R. Conley, Aboozar Mosleh, Amjad Nazzal, Richard A. Soref, Greg Sun, John Tolle, Joe Margetis, Hameed A. Naseem, and Shui-Qing Yu, "Competition of optical transitions between direct and indirect bandgaps in $\text{Ge}_{1-x}\text{Sn}_x$," *Applied Physics Letters*, **105**, 051104 (2014).
- [2] Seyed Amir Ghetmiri, Wei Du, Benjamin R. Conley, Aboozar Mosleh, Amjad Nazzal, Richard A. Soref, Greg Sun, Joe Margetis, John Tolle, Hameed A. Naseem, and Shui-Qing Yu, "Shortwave-infrared photoluminescence from $\text{Ge}_{1-x}\text{Sn}_x$ thin films on silicon", *Journal of Vacuum Science & Technology B*, **32**, 060601 (2014).
- [3] Seyed Amir Ghetmiri, Wei Du, Joe Margetis, Aboozar Mosleh, Larry Cousar, Benjamin R. Conley, Lucas Domulevicz, Amjad Nazzal, Greg Sun, Richard A. Soref, John Tolle, Baohua Li, Hameed A. Naseem, and Shui-Qing Yu, "Direct-bandgap GeSn grown on Silicon with 2230 nm photoluminescence", *Applied Physics Letters*, **105**, 151109 (2014).
- [4] Benjamin R. Conley, Joe Margetis, Wei Du, Huong Tran, Aboozar Mosleh, Seyed Amir Ghetmiri, John Tolle, Greg Sun, Richard Soref, Baohua Li, Hameed A. Naseem, and Shui-Qing Yu, "Si based GeSn photoconductors with a 1.63A/W peak responsivity and a 2.4 μm longwavelength cutoff", *Applied Physics Letters*, **105**, 221117 (2014).

Conference contributions

- [1] Shui-Qing Yu, Wei Du, Benjamin R. Conley, Seyed A. Ghetmiri, Aboozar Mosleh, Thach Pham, Yiyin Zhou, Amjad Nazzal, Greg Sun, Richard A. Soref, Joe Margetis, John Tolle, Baohua Li, and Hameed A. Naseem, "GeSn Photodetector and Light Emitter: Mid-Infrared Devices in Silicon Photonics", **Invited talk**, *SPIE Photonic West*, February 7~12, San Francisco, CA (2015).
- [2] Benjamin R. Conley, Wei Du, Richard A. Soref, Greg Sun, Joe Margetis, John Tolle, Baohua Li, Shui-Qing Yu, "Enhanced gain of GeSn photoconductors by interdigitated electrodes for mid-infrared detection", **Oral presentation**, *SPIE Photonic West*, February 7~12, San Francisco, CA (2015).
- [3] S.-Q. Yu, S. A. Ghetmiri, W. Du, J. Margetis, Y. Zhou, A. Mosleh, S. Al-Kabi, A. Nazzal, G. Sun, R.A. Soref, J. Tolle, B. Li, H.A. Naseem, "Si based GeSn light emitter: mid-infrared device in Si photonics", *Proceedings of SPIE*, vol. **9367**, Silicon Photonics X, 93670R, (February 27 2015).
- [4] Thach Pham, Wei Du, Joe Margetis, Seyed Amir Ghetmiri, Aboozar Mosleh, Greg Sun, Richard A Soref, John Tolle, Hameed A. Naseem, Baohua Li, and Shui-Qing Yu, "Temperature-dependent study of Si-based GeSn photoconductors", *Proceedings of SPIE*, vol. **9367**, Silicon Photonics X, 93670S, (February 27, 2015).



AF SBIR Phase I: Epitaxial Technologies for SiGeSn High Performance Optoelectronics Devices

Dr. Baohua Li (PI), Founder and CEO
Arktonics, LLC
Email: Arktonics@gmail.com
Phone: 479-287-2406

Professor Shui-Qing (Fisher) Yu
Electrical Engineering Department
University of Arkansas
Email: syu@uark.edu
Phone: 479-575-7265
<http://comp.uark.edu/~syu/>



Contract Number: FA9550-14-C-0044
Performance Period: 07/01/2014-04/31/2015



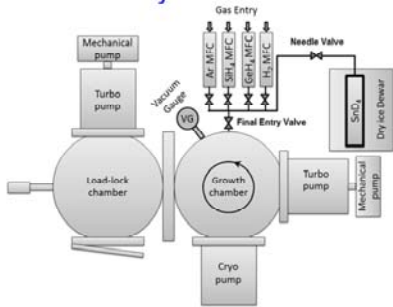
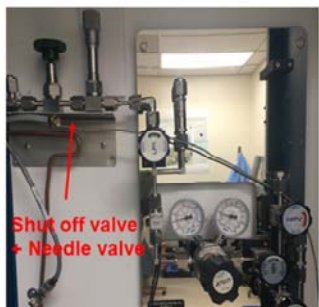
Applied Nano & Bio Photonics Group @ **UARK**



Material growth technique by using UHV-CVD

GeSn/SiGeSn alloys have been grown directly on Si substrate at low temperatures using an cold wall ultra-high vacuum chemical vapor deposition (UHV-CVD) system. The unique growth technique features:

- Both SnCl₄ and SnD₄ as Sn precursors are used (**The only team in the world with this growth capability**);
- No buffer layer needed.

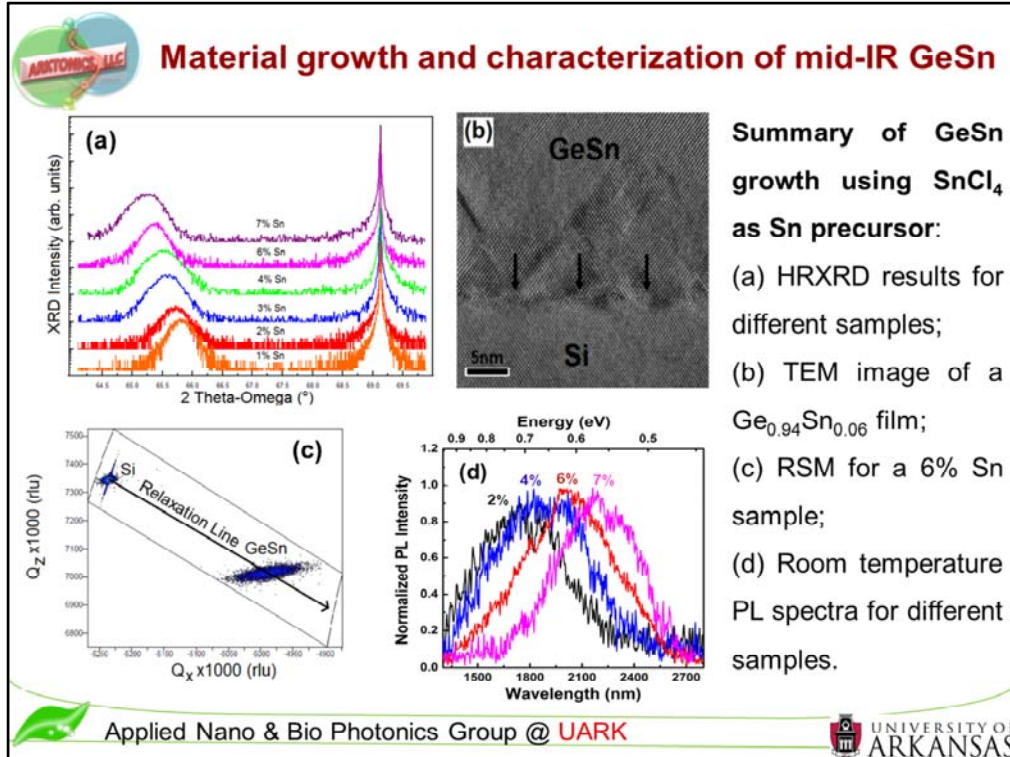
Cold wall UHV-CVD system with SnD₄ in-situ gas mixing. Gases are entered in the chamber through a MFC and a final entry valve. The needle valve is placed after the gas regulators in order to control the SnD₄ flow.

Applied Nano & Bio Photonics Group @ **UARK** UNIVERSITY OF ARKANSAS

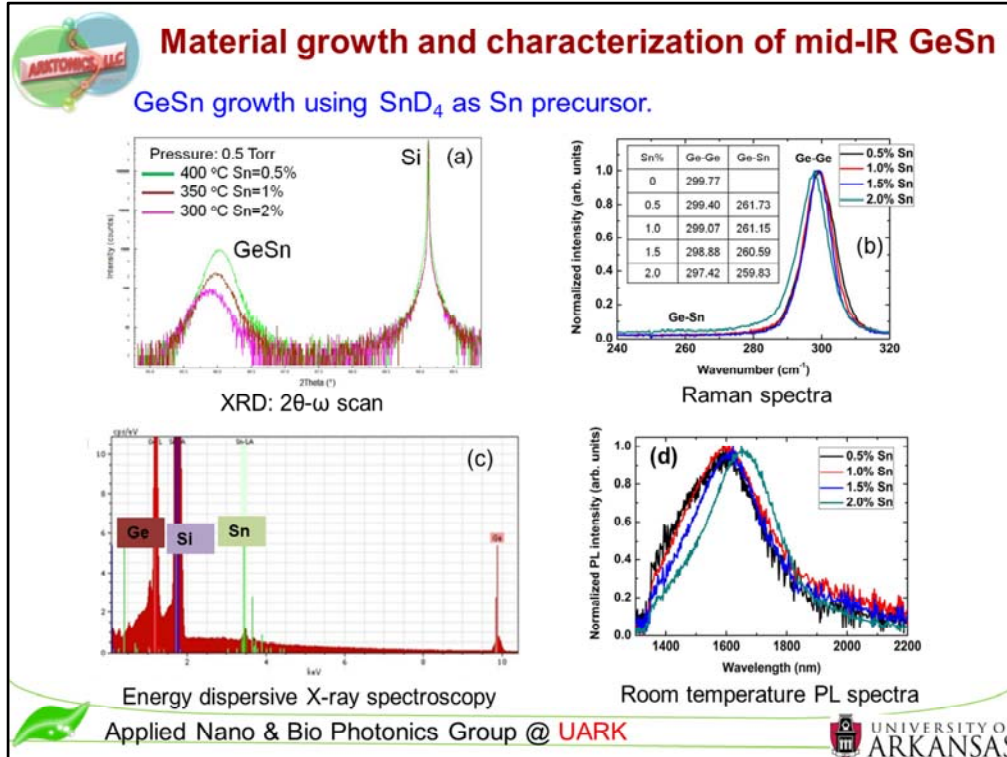
Left: Cold wall UHV-CVD system with SnD₄ in-situ gas mixing. The samples are loaded in the load-lock chamber and after pumping down to 10⁻⁸ Torr pressure it is transferred to the growth chamber. The growth chamber is pumped down with a turbo-molecular pump and a cryogenic pump. Gases enter in the chamber through a MFC and a final entry valve. The SnD₄ gas is kept in dry ice Dewar and is mixed with the gases before entering the chamber through a needle valve. Partial pressure of SnD₄ gas as well as silane, germane and argon are measured by a vacuum gauge.

Right: The needle valve is placed after the gas regulators in order to control the SnD₄ flow.

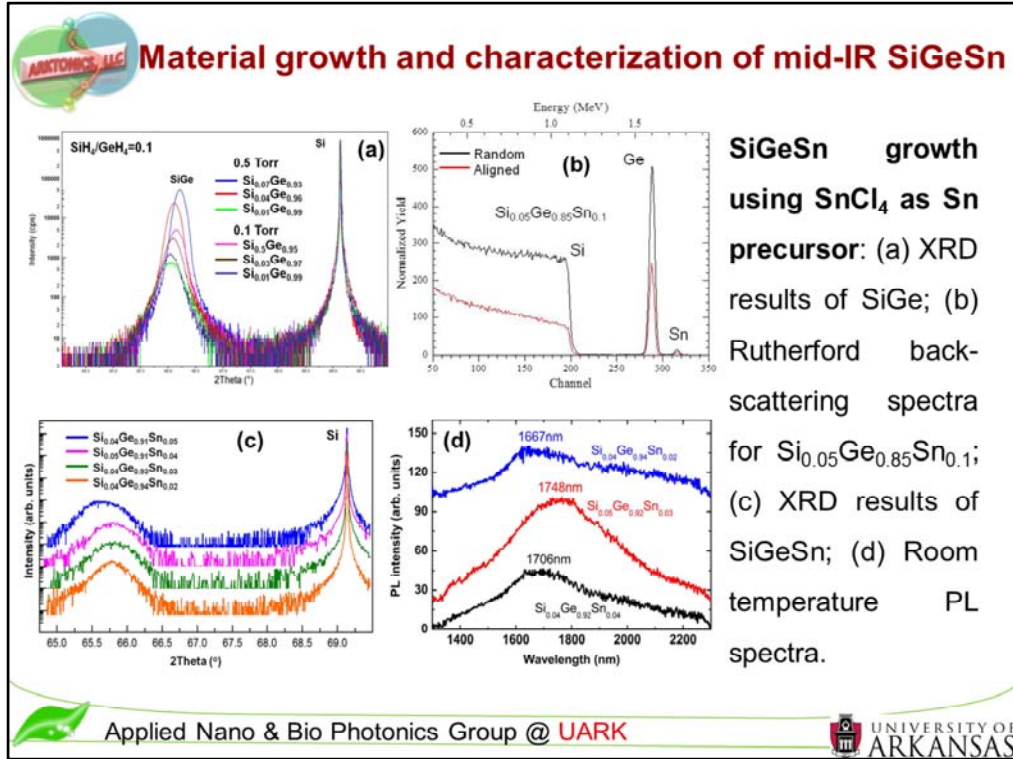
Note: The SnD₄ gas delivering method is different from what ASU is using. Our method is more manufacture friendly. The team tested this method for three months and believes that it is patentable after some further improvement for accurate gas flow control.



- (a) Symmetric (0 0 4) 2θ - ω scan of GeSn films. The gradually shift of GeSn peaks indicates the increase of Sn composition. The results show GeSn with Sn compositions from 1% to 7% (Note, the sample with 5% Sn is not shown due to low quality).
- (b) TEM images of $\text{Ge}_{0.94}\text{Sn}_{0.06}$ film. The arrows show misfit dislocations formed at GeSn/Si interface due to the large lattice mismatch between Si and GeSn.
- (c) The RSM shows that the GeSn layer is strain relaxed grown on Si substrate.
- (d) The normalized PL emission for different samples. As Sn composition increases, the PL peak shifts toward to longer wavelength as a result of bandgap energy reduction.



- (a) The 2θ-ω scan of GeSn thin films grown on Si at the pressures of 0.5 using SnD₄. The growth temperature was also shown in the figures, which was kept below 450 °C to be compatible with a Si complementary metal-oxide-semiconductor (CMOS) process. The GeSn peaks shift toward lower angle in HRXRD indicating the increase of Sn composition.
- (b) Raman spectra of the GeSn films. The shift in Ge-Ge peak is due to the incorporation of Sn in Ge lattice which changes the bond size of Ge-Ge lattice. Ge-Sn peaks are shown at lower wavenumber due to a weaker bond. Inset: peak positions of Ge-Ge and Ge-Sn.
- (c) Energy dispersive X-ray(EDX) spectroscopy of the samples showing Ge and Sn incorporation in the films.
- (d) Room temperature photoluminescence spectra of the GeSn films with Sn compositions from 0.5 to 2 %. Incorporation of Sn has reduced the bangap energy and therefore shifted the PL peak from 1583 nm (0.5% Sn) to 1648 nm (2% Sn).



In order to demonstrate growth of SiGeSn, the study of SiGe growth was firstly conducted (followed by the Sn incorporation to finally achieve SiGeSn growth).

(a) The 2θ - ω scan of SiGe thin films. At low SiH₄/GeH₄ ratio of 0.1, the Si composition varies from 1 to 5 % at pressure of 0.1 Torr and from 1 to 7 % at pressure of 0.5 Torr, respectively.

(b) The ratio of Sn peak heights reveals that only part of Sn atoms are substitutionally incorporated.

(c) 2θ - ω scan of SiGeSn thin films using SnCl₄ as Sn precursor with Sn compositions from 2 to 5 %. The Si composition was kept as 4 % (except a little higher one in Si_{0.05}Ge_{0.91}Sn_{0.04}). As Sn composition increases, the SiGeSn peak gradually shifts toward lower angle. Compared to GeSn samples (the same Sn composition), these peaks are closer to the Si peak due to the Si incorporation. Therefore the incorporation of Si and Sn in Ge can be identified by the spectra behavior.

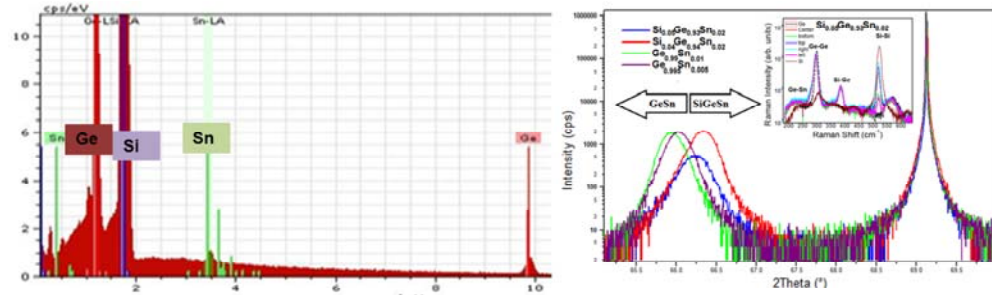
(d) The incorporation of Sn reduces the bandgap energy, which on the contrary is increased by the incorporation of Si. Therefore the PL peak position is determined by both Si and Sn compositions.



Material growth and characterization of mid-IR SiGeSn

The team has also conducted study of SiGeSn growth using SnD₄ as Sn precursor.

- EDX spectroscopy of the samples showing Si, Ge, and Sn incorporation in the films; (left figure)
- Incorporation of Si has resulted in a shift towards higher angles for SiGeSn peaks, which follows the theoretical predication. (right figure)



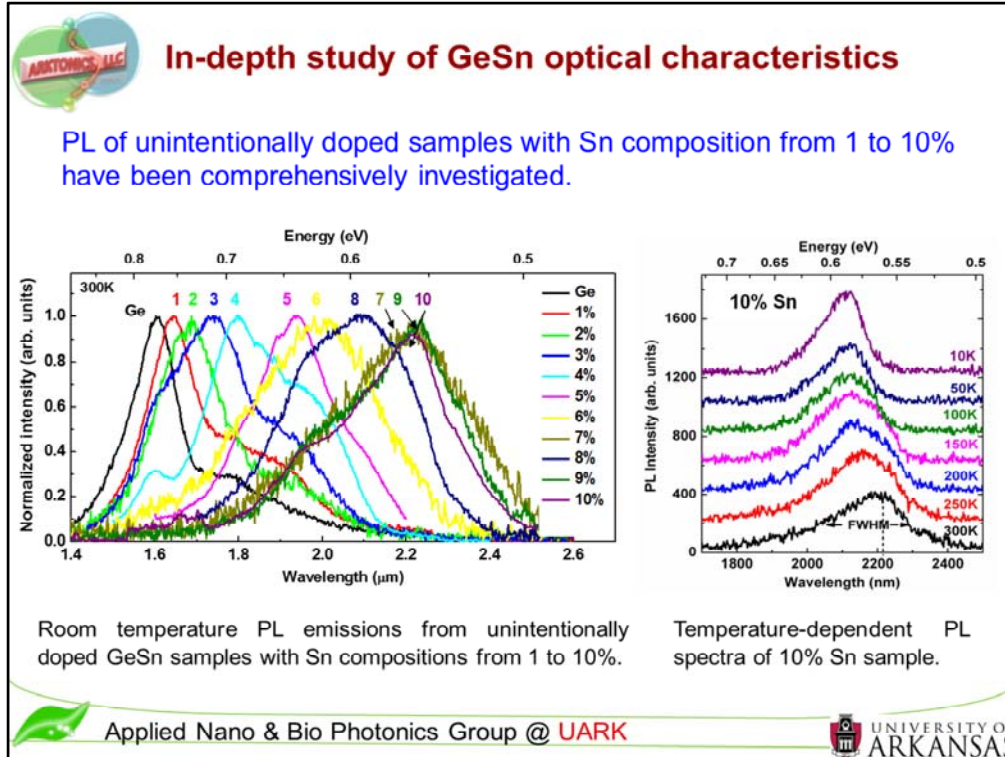
Energy dispersive X-ray(EDX) spectroscopy

The 2θ-ω scans of SiGeSn and GeSn films. Inset shows the Raman spectra of 1% Sn sample.



Applied Nano & Bio Photonics Group @ UARK

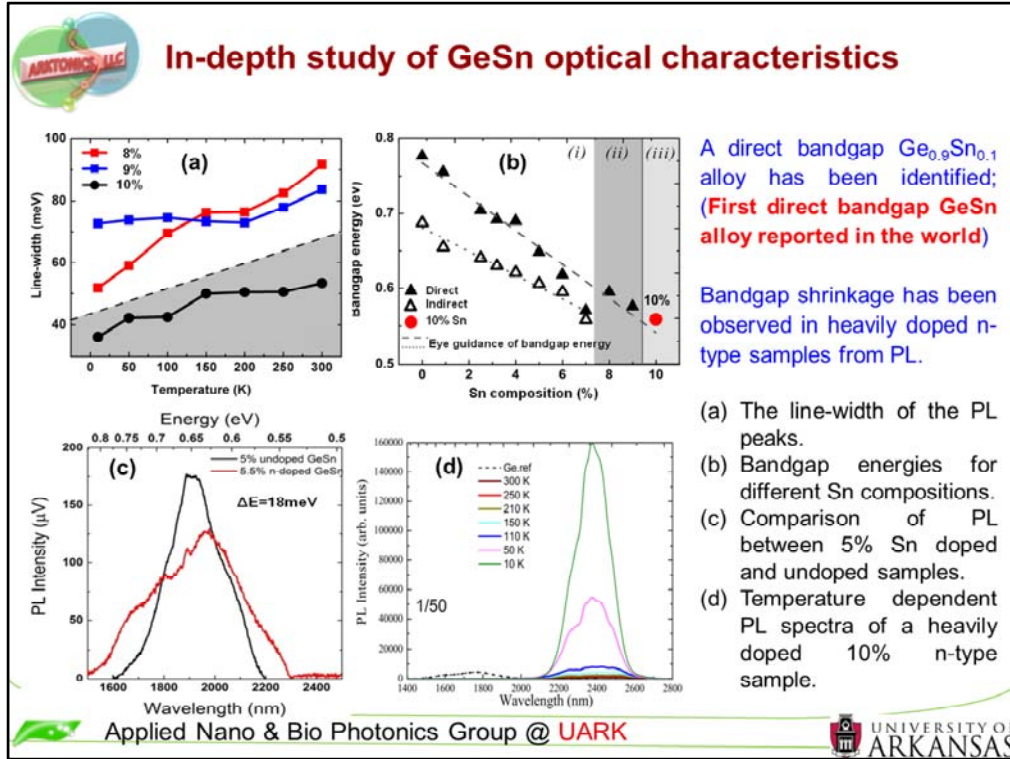




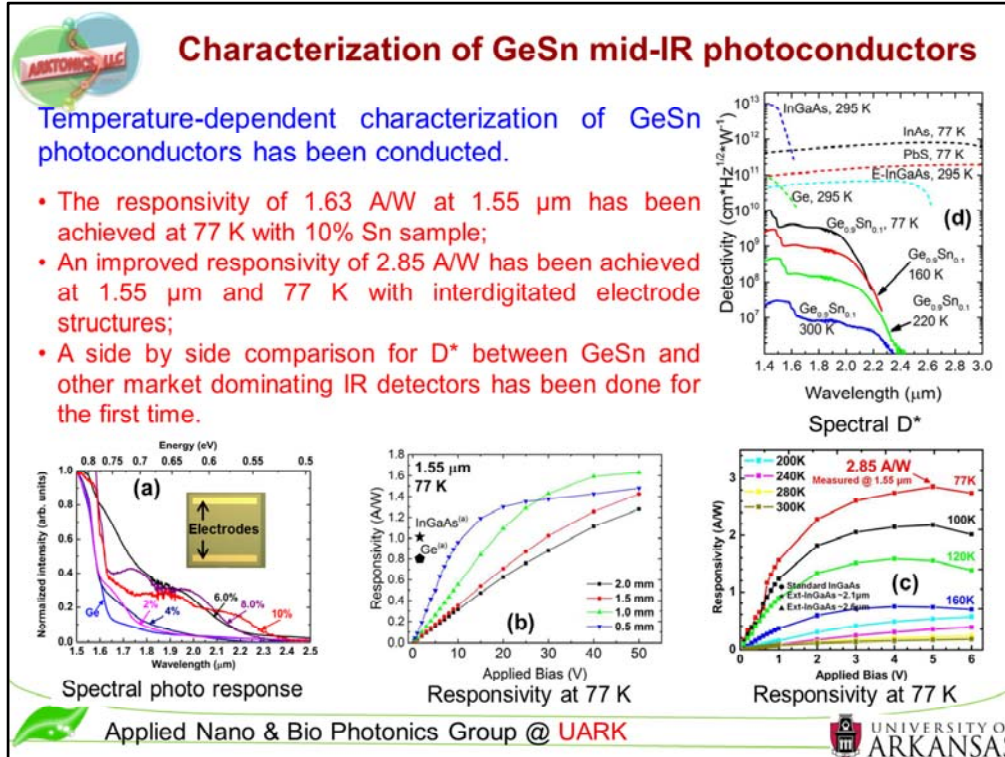
The samples were grown by ASM.

Left: As Sn content increases, the PL peak shifts toward longer wavelength, indicating the narrowed bandgap due to Sn incorporation. The bandgap energy is also affected by strain, therefore 7% Sn sample shows narrower bandgap than 8% Sn sample because of the higher compressive strain of 8% Sn sample. At low Sn composition, two peaks corresponding to direct and indirect bandgap transitions can be identified clearly because of the sufficient energy separation. At higher Sn composition, these two peaks cannot be identified due to the reduced bandgap energy difference, resulting in only a single peak to be observed.

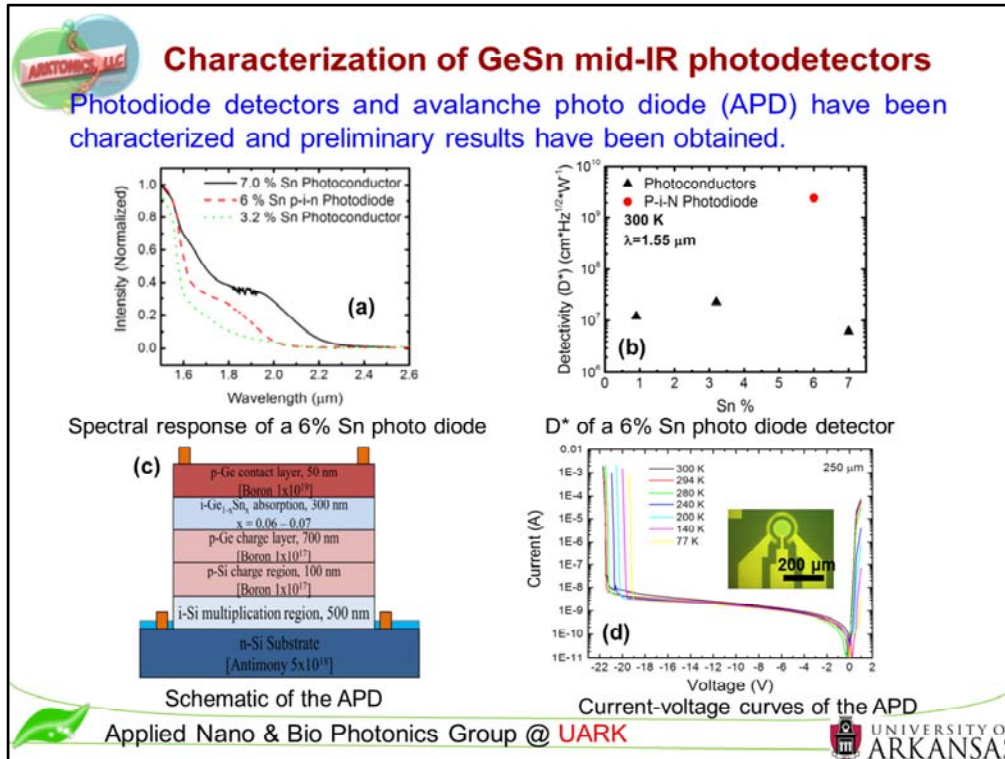
Right: Temperature dependent PL spectra of a 10% GeSn sample in which only a single peak with narrowed line-width was observed. This PL linewidth reduction compared with that of lower Sn composition PL (for example 8 and 9%, not shown in this result).



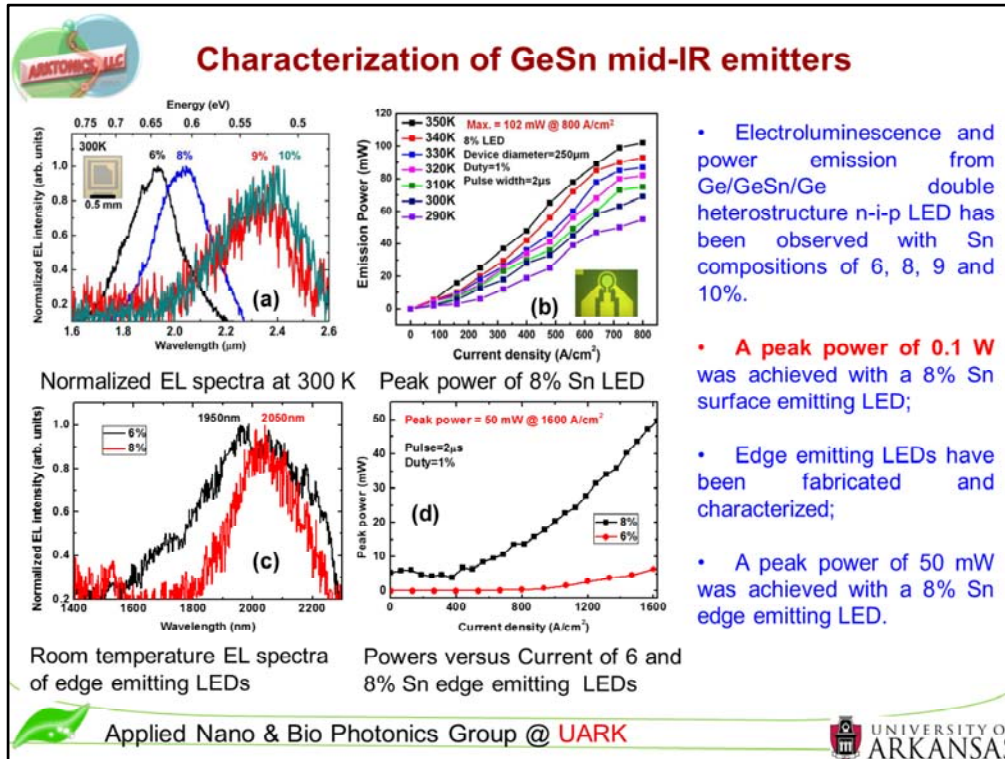
- (a) The line-width of 8 and 9 % Sn samples are nearly twice that of 10% Sn sample at the temperature range from 300 to 100 K, indicating that 10% Sn sample is a direct bandgap material.
- (b) region (i) and (ii) correspond to indirect bandgap material, while region (iii) corresponds to direct bandgap material. The solid and open symbols represent the direct and indirect bandgap energies, respectively. The 10% Sn sample is located in region (iii), which is determined as a direct bandgap material. The solid and dashed lines are eye guidance of direct and indirect bandgap energies, respectively.
- (c) PL spectra of n-type doped GeSn sample and its comparison with unintentionally doped samples with similar Sn composition. The bandgap shrinkage due to the n-type doping is observed as 18, 26, and 61 meV for 5.5, 8.2, and 10% Sn samples, respectively. The figure shows a comparison of PL spectra for 5% doped and undoped samples.
- (d) Temperature dependent PL spectra of a 10% heavily doped n-type GeSn samples. The room temperature PL peak position of the sample is around 2400 nm, which is the longest wavelength reported so far.



- Room temperature spectral photo response of standard photoconductors. As Sn composition increases, the cutoff wavelength shifts towards to longer wavelength and the longest cutoff wavelength of 2.4 μm is observed for a 10 % Sn device.
- Responsivity for standard $\text{Ge}_{0.9}\text{Sn}_{0.1}$ photoconductor measured at 1.55 μm and 77 K. Responsivities of InGaAs and Ge are plotted for comparison. Insets: Optical image of the device.
- Responsivity for $\text{Ge}_{0.9}\text{Sn}_{0.1}$ photoconductor with interdigitated electrode was measured at 1.55 μm and 77 K.
- The spectral D^* for different temperatures shows the comparison of these devices with other mature detector technologies. Note that the D^* of $\text{Ge}_{0.9}\text{Sn}_{0.1}$ is only one order-of-magnitude lower than that of Ge, extended-InGaAs, and PbS detectors in the short wavelength IR range.



- (a) Spectral response up to 2 μm has been observed for a 6 % GeSn photo diode and the response was compared with two different photoconductors (3.2 and 7% Sn).
- (b) GeSn photodiode has much lower dark current (at reverse applied voltage) compared to photoconductor, the D^* of photo diode is two order of magnitude higher than that of photoconductor.
- (c) Schematic of the cross-section for the APD device. Absorption-Charge-Multiplication (SACM) structure has been used, which takes advantage of the excellent optical absorption of GeSn at mid-IR range and the outstanding carrier multiplication properties of Si.
- (d) The preliminary testing results of the temperature dependent I-V curves have shown device breakdown behavior.



- Electroluminescence and power emission from Ge/GeSn/Ge double heterostructure n-i-p LED has been observed with Sn compositions of 6, 8, 9 and 10%.

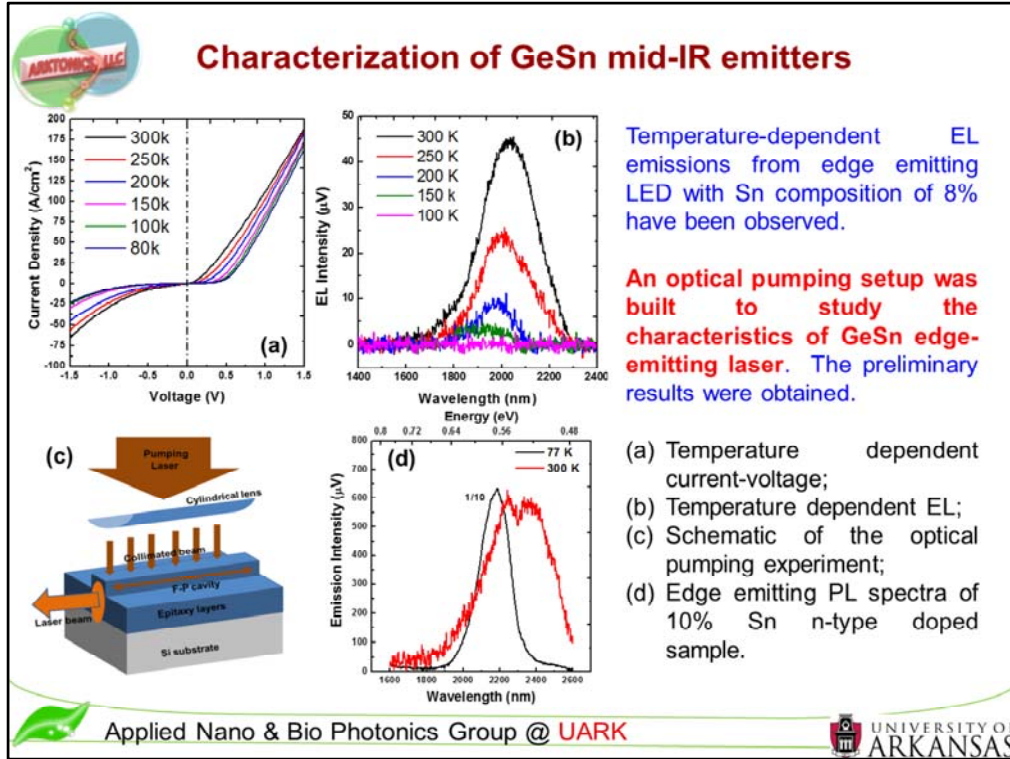
- A peak power of 0.1 W was achieved with a 8% Sn surface emitting LED;

- Edge emitting LEDs have been fabricated and characterized;

- A peak power of 50 mW was achieved with a 8% Sn edge emitting LED.

- Normalized EL spectra for surface emitting LEDs at room temperature. As Sn composition increases, the EL peak position shifts to longer wavelength. The EL emission at 2380 nm was observed from 10% Sn LED. For the devices with 9 and 10% Sn LEDs the PbS detector (cut-off at 3 μm) is applied to measure the spectra, whose signal-to-noise ratio is lower than that of the InGaAs detector (cut-off at 2.3 μm) which is used to measure the EL of LEDs with 6 and 8% Sn LEDs.
- The emission power measurement has been performed by using a pulsed current source in order to eliminate the contribution from Joule heating. The peak emission power of 0.1 W has been achieved for a 8% Sn surface emitting LED at an injection of 800 A/cm^2 and a working temperature of 350 K.
- Normalized EL spectra of 6 and 8% Sn edge emitting LEDs at room temperature. These results are consistent with surface emitting LED.
- The peak emission power of 50 mW has been achieved for a 8% Sn edge emitting LED at an injection of 1600 A/cm^2 .

Note: (Results are not shown here) Temperature-dependent EL emissions from the surface emitting LEDs with Sn compositions of 6 and 8% have been investigated. The blue-shift of EL peak with decreased temperature has been observed.



- (a) The current-voltage characteristic. The clearly rectifying behavior is observed at temperatures from 80 to 300 K.
- (b) The temperature-dependent EL spectra of $\text{Ge}_{0.92}\text{Sn}_{0.08}$ LED from 80 to 300 K at an injection level of 600 A/cm^2 . The peak shift to shorter wavelength at lower temperature is observed.
- (c) The team has built an optical pumping setup in order to study the GeSn lasing characteristics. The mirrors of the F-P cavity was formed by lapping the Si substrates and then cleaving of end facets. The fs Ti:Sapphire laser which could provide sufficiently high pumping power was used as pump laser.
- (d) As temperature decreases, the PL intensity dramatically increases and the peak becomes symmetric, indicating the lasing can be expected at lower temperature with improved light confinement. Further study is ongoing.

MATERIAL INSPECTION AND RECEIVING REPORT

Form Approved
OMB No. 0704-0248

The public reporting burden for this collection of information is estimated to average 30 minutes per response, including the time for reviewing instructions, searching existing data sources, gathering and maintaining the data needed, and completing and reviewing the collection of information. Send comments regarding this burden estimate or any other aspect of this collection of information, including suggestions for reducing the burden, to Department of Defense, Washington Headquarters Services, Directorate for Information Operations and Reports (0704-0248), 1215 Jefferson Davis Highway, Suite 1204, Arlington, VA 22202-4302. Respondents should be aware that notwithstanding any other provision of law, no person shall be subject to any penalty for failing to comply with a collection of information if it does not display a currently valid OMB control number.

PLEASE DO NOT RETURN YOUR COMPLETED FORM TO THE ABOVE ADDRESS.
SEND THIS FORM IN ACCORDANCE WITH THE INSTRUCTIONS CONTAINED IN THE DFARS, APPENDIX F-401.

1. PROCUREMENT INSTRUMENT IDENTIFICATION (CONTRACT) NO. FA9550-14-C-0044		ORDER NO.	6. INVOICE NO./DATE 0003/4/21/2015		7. PAGE OF 1 1	8. ACCEPTANCE POINT DESTINATION
2. SHIPMENT NO. FAY0004Z	3. DATE SHIPPED 4/21/2015	4. B/L TCN		5. DISCOUNT TERMS N/A		
9. PRIME CONTRACTOR CODE ARKTONICS, LLC 1339 S PINNACLE DR FAYETTEVILLE AR 72701-7781			10. ADMINISTERED BY CODE S4402A DCMA DALLAS 600 NORTH PEARL STREET DALLAS TX 75201-2812 DCMADALLASCASDIRECTORY@DCMA.MIL			
11. SHIPPED FROM (If other than 9) CODE		FOB:	12. PAYMENT WILL BE MADE BY CODE HQ0339 DFAS COLUMBUS CENTER DFAS-CO/WEST ENTITLEMENT OPS PO BOX 182381 COLUMBUS OH 43218-2381			
13. SHIPPED TO CODE FA9550 DR GERNOT POMRENKE, AFOSR/RTD AIR FORCE OFFICE OF SCIENTIFIC RESEARCH 875 N RANDOLPH STREET, STE 325, ROOM 3112 ARLINGTON, VA 22203			14. MARKED FOR CODE			

15. ITEM NO.	16. STOCK/PART NO. (Indicate number of shipping containers - type of container - container number.)	DESCRIPTION	17. QUANTITY SHIP/REC'D*	18. UNIT	19. UNIT PRICE	20. AMOUNT
0001	AC	Final Technical Report & Invention Report SHIPPING CONTAINERS - 1 CONTAINER TYPE - ENVELOPE CONTAINER NO. - 003	1	LO	40,000.000	40,000.00

21. CONTRACT QUALITY ASSURANCE a. ORIGIN <input type="checkbox"/> CQA <input type="checkbox"/> ACCEPTANCE of listed items has been made by me or under my supervision and they conform to contract, except as noted herein or on supporting documents.		b. DESTINATION <input type="checkbox"/> CQA <input type="checkbox"/> ACCEPTANCE of listed items has been made by me or under my supervision and they conform to contract, except as noted herein or on supporting documents.		22. RECEIVER'S USE Quantities shown in column 17 were received in apparent good condition except as noted.	
DATE _____ SIGNATURE OF AUTHORIZED GOVERNMENT REPRESENTATIVE _____		DATE _____ SIGNATURE OF AUTHORIZED GOVERNMENT REPRESENTATIVE _____		DATE RECEIVED _____ SIGNATURE OF AUTHORIZED GOVERNMENT REPRESENTATIVE _____	
TYPED NAME: TITLE: MAILING ADDRESS:		TYPED NAME: TITLE: MAILING ADDRESS:		TYPED NAME: TITLE: MAILING ADDRESS:	
COMMERCIAL TELEPHONE NUMBER:		COMMERCIAL TELEPHONE NUMBER:		COMMERCIAL TELEPHONE NUMBER:	

* If quantity received by the Government is the same as quantity shipped, indicate by (X) mark; if different, enter actual quantity received below quantity shipped and encircle.

23. CONTRACTOR USE ONLY
 Research entitled " Epitaxial Technologies for SiGenSn High Performance Optoelectronic Devices" dated 22 January 2014 is conducted. DD Form 250 is submitted through WAWF system. DD Form 250, Final Technical Report, and Invention Report DD Form 882 for the performance period 01 July 2014 through 31 March 2015 are shipped to CAO with code S4420A. They are also submitted to <http://afosr.reports.sgizmo.com/s3> and to the program manager (gernot.pomrenke@us.af.mil). In addition, Invention Report DD Form 882 is submitted to AFOSR/PKC (afrl.afosr.pkcontracting@us.af.mil).

REPORT OF INVENTIONS AND SUBCONTRACTS
(Pursuant to "Patent Rights" Contract Clause/ See Instructions on back)

Form Approved
 OMB No. 9000-0095
 Expires Jan 31, 2008

The public reporting burden for this collection of information is estimated to average 1 hour per response, including the time for reviewing instructions, searching existing data sources, gathering and maintaining the data needed, and completing and reviewing the collection of information. Send comments regarding this burden estimate or any other aspect of this collection of information, including suggestions for reducing the burden, to the Department of Defense, Executive Service Directorate (9000-0095). Respondents should be aware that notwithstanding any other provision of law, no person shall be subject to any penalty for failing to comply with a collection of information if it does not display a currently valid OMB control number.

PLEASE DO NOT RETURN YOUR COMPLETED FORM TO THE ABOVE ORGANIZATION. RETURN COMPLETED FORM TO THE CONTRACTING OFFICER.

1. a. NAME OF CONTRACTOR/SUBCONTRACTOR Arkonics, LLC		c. CONTRACT NUMBER FA9550-14-C-0044		2. a. NAME OF GOVERNMENT PRIME CONTRACTOR Arkonics, LLC		c. CONTRACT NUMBER FA9550-14-C-0044		3. TYPE OF REPORT (X one)	
b. ADDRESS (include ZIP Code) 1339 S. Pinnacle Dr. Fayetteville, AR 72701		d. AWARD DATE (YYYYMMDD) 20140701		b. ADDRESS (include ZIP Code) 1339 S. Pinnacle Dr. Fayetteville, AR 72701		d. AWARD DATE (YYYYMMDD) 20140701		a. INTERIM <input type="checkbox"/> b. FINAL <input checked="" type="checkbox"/>	
						4. REPORTING PERIOD (YYYYMMDD)		a. FROM 20140701 b. TO 20150331	

SECTION I - SUBJECT INVENTIONS

5. "SUBJECT INVENTIONS" REQUIRED TO BE REPORTED BY CONTRACTOR/SUBCONTRACTOR (If "None," so state)	NAME(S) OF INVENTOR(S) <i>(Last, First, Middle Initial)</i>	TITLE OF INVENTION(S)	DISCLOSURE NUMBER, PATENT APPLICATION SERIAL NUMBER OR PATENT NUMBER	ELECTION TO FILE PATENT APPLICATIONS (X)				CONFIRMATORY INSTRUMENT OR ASSIGNMENT FORWARDED TO CONTRACTING OFFICER (X)	
				(1) UNITED STATES		(2) FOREIGN		(1) YES (a) YES (a) NO (b) NO	
None	a.	b.	c.	(a) YES	(b) NO	(a) YES	(b) NO	(a) YES	(b) NO

SECTION II - SUBCONTRACTS (Containing a "Patent Rights" clause)

6. SUBCONTRACTS AWARDED BY CONTRACTOR/SUBCONTRACTOR (If "None," so state)									
NAME OF SUBCONTRACTOR(S)	ADDRESS (include ZIP Code)	SUBCONTRACT NUMBER(S)	FAR "PATENT RIGHTS"		DESCRIPTION OF WORK TO BE PERFORMED UNDER SUBCONTRACT(S)	SUBCONTRACT DATES (YYYYMMDD)		SUBCONTRACT NUMBER(S)	ESTIMATED COMPLETION
			(1) CLAUSE NUMBER	(2) DATE (YYYYMM)		(1) AWARD	(2) ESTIMATED COMPLETION		
University of Arkansas	210 Administration Building, Fayetteville, AR 72701-1201	None	52.227	201407	UHV-CVD Growth of SiGeSn and Development of GeSn Detectors and Emitters	20140701	20150331		

SECTION III - CERTIFICATION

7. CERTIFICATION OF REPORT BY CONTRACTOR/SUBCONTRACTOR (Not required if "X" as appropriate)

I certify that the reporting party has procedures for prompt identification and timely disclosure of "Subject Inventions," that such procedures have been followed and that all "Subject Inventions" have been reported.

SMALL BUSINESS or NONPROFIT ORGANIZATION

a. NAME OF AUTHORIZED CONTRACTOR/SUBCONTRACTOR OFFICIAL - <i>(Last, First, Middle Initial)</i> Li, Baohua	b. TITLE President of Arkonics, LLC	c. SIGNATURE 	d. DATE SIGNED 20150417
---	---	---	-----------------------------------

REPORT OF INVENTIONS AND SUBCONTRACTS
(Pursuant to "Patent Rights" Contract Clause) (See Instructions on back)

The public reporting burden for this collection of information is estimated to average 1 hour per response, including the time for reviewing instructions, searching existing data sources, gathering and maintaining the data needed, and completing and reviewing the collection of information. Send comments regarding this burden estimate or any other aspect of this collection of information, including suggestions for reducing the burden, to the Department of Defense, Executive Services Directorate (9000-0095). Respondents should be aware that notwithstanding any other provision of law, no person shall be subject to any penalty for failing to comply with a collection of information if it does not display a currently valid OMB control number.

PLEASE DO NOT RETURN YOUR COMPLETED FORM TO THE ABOVE ORGANIZATION. RETURN COMPLETED FORM TO THE CONTRACTING OFFICER.

1. a. NAME OF CONTRACTOR/SUBCONTRACTOR University of Arkansas		c. CONTRACT NUMBER FA9550-14-C-0044	
b. ADDRESS (Include ZIP Code) 210 Administration Building, Fayetteville, AR 72701-1201		d. AWARD DATE (YYYYMMDD) 20140701	
2. a. NAME OF GOVERNMENT PRIME CONTRACTOR Arktionics, LLC		c. CONTRACT NUMBER FA9550-14-C-0044	
b. ADDRESS (Include ZIP Code) 1339 S. Pinnacle Dr. Fayetteville, AR 72701		d. AWARD DATE (YYYYMMDD) 20140701	
3. TYPE OF REPORT (X one)		a. INTERIM <input type="checkbox"/>	
		b. FINAL <input checked="" type="checkbox"/>	
4. REPORTING PERIOD (YYYYMMDD)		a. FROM 20140701	
		b. TO 20150331	

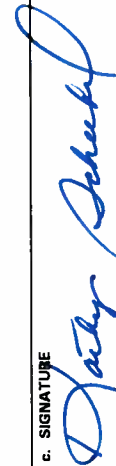
SECTION I - SUBJECT INVENTIONS

5. "SUBJECT INVENTIONS" REQUIRED TO BE REPORTED BY CONTRACTOR/SUBCONTRACTOR (If "None," so state)		ELECTION TO FILE PATENT APPLICATIONS (X)		CONFIRMATORY INSTRUMENT OR ASSIGNMENT FORWARDED TO CONTRACTING OFFICER (X)	
NAME(S) OF INVENTOR(S) (Last, First, Middle Initial)	TITLE OF INVENTION(S)	DISCLOSURE NUMBER, PATENT APPLICATION SERIAL NUMBER OR PATENT NUMBER		ELECTED FOREIGN COUNTRIES IN WHICH A PATENT APPLICATION WILL BE FILED	
		(1) UNITED STATES	(2) FOREIGN	(1) YES (a)	(2) NO (b)
None		(a) YES	(b) NO	(a) YES	(b) NO
f. EMPLOYER OF INVENTOR(S) NOT EMPLOYED BY CONTRACTOR/SUBCONTRACTOR					
(1) (a) NAME OF INVENTOR (Last, First, Middle Initial)	(2) (a) NAME OF INVENTOR (Last, First, Middle Initial)	(1) TITLE OF INVENTION		(2) FOREIGN COUNTRIES OF PATENT APPLICATION	
(b) NAME OF EMPLOYER	(b) NAME OF EMPLOYER				
(c) ADDRESS OF EMPLOYER (Include ZIP Code)	(c) ADDRESS OF EMPLOYER (Include ZIP Code)				

SECTION II - SUBCONTRACTS (Containing a "Patent Rights" clause)

6. SUBCONTRACTS AWARDED BY CONTRACTOR/SUBCONTRACTOR (If "None," so state)		FAR "PATENT RIGHTS"		SUBCONTRACT DATES (YYYYMMDD)	
NAME OF SUBCONTRACTOR(S)	ADDRESS (Include ZIP Code)	SUBCONTRACT NUMBER(S)	(1) CLAUSE NUMBER	(2) DATE (YYYYMM)	(1) AWARD
a.					
b.					
None					

SECTION III - CERTIFICATION

7. CERTIFICATION OF REPORT BY CONTRACTOR/SUBCONTRACTOR (Not required if: (X as appropriate))		<input checked="" type="checkbox"/> NONPROFIT ORGANIZATION	
I certify that the reporting party has procedures for prompt identification and timely disclosure of "Subject Inventions," that such procedures have been followed and that all "Subject Inventions" have been reported.		d. DATE SIGNED 4/17/15	
a. NAME OF AUTHORIZED CONTRACTOR/SUBCONTRACTOR OFFICIAL (Last, First, Middle Initial) Scheibel, Kathy	b. TITLE Assistant Director, Research & Sponsored Programs	c. SIGNATURE 	

Invention Report:

Primary contractor Arktonics, LLC does not file any invention or patent.

Subcontractor University of Arkansas does not file any invention or patent.



1.

1. Report Type

Final Report

Primary Contact E-mail

Contact email if there is a problem with the report.

Arktonics@gmail.com

Primary Contact Phone Number

Contact phone number if there is a problem with the report

479-287-2406

Organization / Institution name

Arktonics, LLC

Grant/Contract Title

The full title of the funded effort.

(AF SBIR Phase I) Epitaxial Technologies for SiGeSn High Performance Optoelectronic Devices

Grant/Contract Number

AFOSR assigned control number. It must begin with "FA9550" or "F49620" or "FA2386".

FA9550-14-C-0044

Principal Investigator Name

The full name of the principal investigator on the grant or contract.

Baohua Li

Program Manager

The AFOSR Program Manager currently assigned to the award

Gernot Pomrenke

Reporting Period Start Date

07/01/2014

Reporting Period End Date

03/31/2015

Abstract

The main content of this report includes i) Growth of mid-IR GeSn/SiGeSn materials using Ultra-high-vacuum Chemical Vapor Deposition, ii) In-depth characterizations of GeSn materials using different techniques, and iii) Development of GeSn mid-IR detectors and emitters. For material growth work, buffer free growth of Ge, SiGe, SiSn, GeSn, and SiGeSn on Si substrate has been demonstrated. Both SnCl₄ and SnD₄ are used as Sn precursors for GeSn and SiGeSn growth. So far 276 wafers have been grown. The GeSn/SiGeSn material characterizations have been performed via X-ray diffraction, Raman, ellipsometry, Rutherford backscattering spectra (RBS), and high resolution transmission electron microscopy (TEM). The XRD result clearly shows GeSn, SiGe, and SiGeSn peaks indicating the success of the growth. The highest Sn incorporation is determined to be 7% for GeSn materials and the substitutional incorporation of Sn for SiGeSn varies from 2% to 5%. The reciprocal space map shows that the as-grown GeSn layers are relaxed. The TEM image shows that the misfit dislocations are localized at the interface between Si and epitaxy layer. Room temperature photoluminescence (PL) from

DISTRIBUTION A: Distribution approved for public release

GeSn and SiGeSn samples have been observed. The PL peak positions agree well with the theoretical prediction. High quality GeSn samples grown by ASM have been comprehensively characterized. A direct bandgap Ge_{0.9}Sn_{0.1} alloy has been identified which is the first report of direct bandgap GeSn alloy. Moreover, bandgap shrinkage has been observed in heavily doped n-type samples. GeSn samples have been fabricated into photoconductive detectors, avalanche photo diodes, and light-emitting diodes (LEDs) and in-depth study has been conducted. The responsivity of 1.63 A/W at 1.55 μm has been achieved with a Ge_{0.9}Sn_{0.1} photoconductor at 77 K, which is higher than that of market dominating Ge and InGaAs detectors. The team has done for the first time a side by side comparison for specific detectivity (D*) between GeSn and other market dominating infrared detectors in short wavelength infrared range. An improved responsivity of 2.85 A/W has been achieved on Ge_{0.9}Sn_{0.1} photoconductors at 1.55 μm and 77 K by using an interdigitated electrode design. Temperature-dependent electroluminescence and power output from Ge/GeSn/Ge double heterostructure n-i-p surface and edge emitting LEDs have been studied for samples with Sn composition up to 10%. The peak emission power of 0.1 W (8% Sn surface emitting LED at 800 A/cm² and 350 K) and 50 mW (8% Sn edge emitting LED at 1600 A/cm² and 300 K) have been achieved, respectively. An optical pumping characterization system for edge-emitting lasers has been constructed and the preliminary results from a 11% GeSn sample have been obtained showing the promise of achieving lasing at low temperatures.

Distribution Statement

This is block 12 on the SF298 form.

Distribution A - Approved for Public Release

Explanation for Distribution Statement

If this is not approved for public release, please provide a short explanation. E.g., contains proprietary information.

SF298 Form

Please attach your SF298 form. A blank SF298 can be found [here](#). Please do not password protect or secure the PDF. The maximum file size for an SF298 is 50MB.

[SF298.pdf](#)

Upload the Report Document. File must be a PDF. Please do not password protect or secure the PDF. The maximum file size for the Report Document is 50MB.

[Final Technical Report and DD Form 250 and DD Form 882 for Contract Number FA955014C0044.pdf](#)

Upload a Report Document, if any. The maximum file size for the Report Document is 50MB.

Archival Publications (published) during reporting period:

Journal papers

- [1] Wei Du, Seyed A. Ghetmiri, Benjamin R. Conley, Aboozar Mosleh, Amjad Nazzal, Richard A. Soref, Greg Sun, John Tolle, Joe Margetis, Hameed A. Naseem, and Shui-Qing Yu, "Competition of optical transitions between direct and indirect bandgaps in Ge_{1-x}Sn_x," Applied Physics Letters, 105, 051104 (2014).
- [2] Seyed Amir Ghetmiri, Wei Du, Benjamin R. Conley, Aboozar Mosleh, Amjad Nazzal, Richard A. Soref, Greg Sun, Joe Margetis, John Tolle, Hameed A. Naseem, and Shui-Qing Yu, "Shortwave-infrared photoluminescence from Ge_{1-x}Sn_x thin films on silicon", Journal of Vacuum Science & Technology B, 32, 060601 (2014).
- [3] Seyed Amir Ghetmiri, Wei Du, Joe Margetis, Aboozar Mosleh, Larry Cousar, Benjamin R. Conley, Lucas Domulevicz, Amjad Nazzal, Greg Sun, Richard A. Soref, John Tolle, Baohua Li, Hameed A. Naseem, and Shui-Qing Yu, "Direct-bandgap GeSn grown on Silicon with 2230 nm photoluminescence", Applied Physics Letters, 105, 151109 (2014).
- [4] Benjamin R. Conley, Joe Margetis, Wei Du, Huong Tran, Aboozar Mosleh, Seyed Amir

DISTRIBUTION A: Distribution approved for public release

Ghetmiri, John Tolle, Greg Sun, Richard Soref, Baohua Li, Hameed A. Naseem, and Shui-Qing Yu, "Si based GeSn photoconductors with a 1.63A/W peak responsivity and a 2.4µm longwavelength cutoff", Applied Physics Letters, 105, 221117 (2014).

Conference contributions

[1] Shui-Qing Yu, Wei Du, Benjamin R. Conley, Seyed A. Ghetmiri, Aboozar Mosleh, Thach Pham, Yiyin Zhou, Amjad Nazzal, Greg Sun, Richard A. Soref, Joe Margetis, John Tolle, Baohua Li, and Hameed A. Naseem, "GeSn Photodetector and Light Emitter: Mid-Infrared Devices in Silicon Photonics", Invited talk, SPIE Photonic West, February 7~12, San Francisco, CA (2015).

[2] Benjamin R. Conley, Wei Du, Richard A. Soref, Greg Sun, Joe Margetis, John Tolle, Baohua Li, Shui-Qing Yu, "Enhanced gain of GeSn photoconductors by interdigitated electrodes for mid-infrared detection", Oral presentation, SPIE Photonic West, February 7~12, San Francisco, CA (2015).

[3] S.-Q. Yu, S. A. Ghetmiri, W. Du, J. Margetis, Y. Zhou, A. Mosleh, S. Al-Kabi, A. Nazzal, G. Sun, R.A. Soref, J. Tolle, B. Li, H.A. Naseem, "Si based GeSn light emitter: mid-infrared device in Si photonics", Proceedings of SPIE, vol. 9367, Silicon Photonics X, 93670R, (February 27 2015).

[4] Thach Pham, Wei Du, Joe Margetis, Seyed Amir Ghetmiri, Aboozar Mosleh, Greg Sun, Richard A Soref, John Tolle, Hameed A. Naseem, Baohua Li, and Shui-Qing Yu, "Temperature-dependent study of Si-based GeSn photoconductors", Proceedings of SPIE, vol. 9367, Silicon Photonics X, 93670S, (February 27, 2015).

Changes in research objectives (if any):

Change in AFOSR Program Manager, if any:

Extensions granted or milestones slipped, if any:

AFOSR LRIR Number

LRIR Title

Reporting Period

Laboratory Task Manager

Program Officer

Research Objectives

Technical Summary

Funding Summary by Cost Category (by FY, \$K)

	Starting FY	FY+1	FY+2
Salary			
Equipment/Facilities			
Supplies			
Total			

Report Document

Report Document - Text Analysis

Report Document - Text Analysis

Appendix Documents

2. Thank You

E-mail user

Apr 21, 2015 14:09:35 Success: Email Sent to: Arktonics@gmail.com